Article

Not peer-reviewed version

Long Exposure to Salt Stress Leads to Stronger Damage in Chloroplast Ultrastructure and its Functionality than the Stomatal Function in *Jatropha curcas*

Marcelo F. Pompelli *, Jaqueline Dias Pereira, Juan de Dios Jaraba-Navas, Alfredo Jarma-Orozco, Luis Alfonso Rodriguez-Paez, Yirlis Yadeth Pineda-Rodriguez, Wagner L. Araújo

Posted Date: 4 July 2023

doi: 10.20944/preprints202307.0048.v1

Keywords: purging nut; scanning electron microscopy; transmission electron microscopy; chloroplast ultrastructure; NaCl long exposition time; hydraulic conductivity

Article

Long Exposure to Salt Stress Leads to Stronger Damage in Chloroplast Ultrastructure and its Functionality than the Stomatal Function in *Jatropha curcas*

Marcelo F. Pompelli [1,*], Jaqueline Dias Pereira [2], Juan de Dios Jaraba-Navas [1], Alfredo Jarma-Orozco [1], Luis Alfonso Rodríguez-Paez [1], Yirlis Yadeth Pineda-Rodriguez [1] and Wagner L. Araújo [3]

[1] Facultad de Ciencias Agricolas, Universidad de Córdoba, Montería, Córdoba, Colombia. Zipcode 360002; jjaraba@correo.unicordoba.edu.co (J.D.J.-N.); ajarma@correo.unicordoba.edu.co (A.J.-O.); larguez@fca.edu.co (L.A.R.-P.); yadeth@fca.edu.co (Y.Y.P.-R.)

[2] Universidade Federal de Viçosa, Rio Paranaíba Campus, Rio Paranaíba, MG, Brazil, Zipcode 38810-000; jaqueline.dias@ufv.br (J.D.P.)

[3] Universidade Federal de Viçosa, Viçosa, Departamento de Biologia Vegetal, Viçosa, MG, Brazil, Zipcode 56570-000; wlaraujo@ufv.br (W.L.A.)

* Correspondence: marcelo@fca.edu.co

Abstract: As sessile organisms, plants face a wide range of abiotic stresses, with salinity being a prominent constraint affecting their growth, development, and productivity, particularly in arid and semi-arid regions. This study focused on understanding how salinity impacts *Jatropha curcas*, an important oilseed plant for biodiesel production. By examining the anatomy and ultrastructure of stomata and chloroplasts, we investigated the effects of prolonged salinity stress on *J. curcas*. This stress led to changes in stomatal density, stomatal index, and ostiole aperture, which case an imbalance of water conductivity in the xylem. Through transmission electron microscopy, we explored the subcellular organization of *J. curcas* chloroplasts and their contribution to plant photosynthetic efficiency, providing insights into their role in this process. Notably, salinity treatment resulted in a significant increase in starch granules accumulation, leading to impaired the granal and stromal grana lamellae, destroying this ultrastructure. Our findings indicate that the anatomy and ultrastructure of chloroplasts play a crucial role in influencing photosynthetic efficiency and hydraulic conductivity. This study offers new perspectives on the structure and function of chloroplasts in *J. curcas*, presenting innovative opportunities to develop strategies that enhance biofuel production in areas with high soil salinity.

Keywords: purging nut; scanning electron microscopy; transmission electron microscopy; chloroplast ultrastructure; NaCl long exposition time; hydraulic conductivity

1. Introduction

Salinity is an environmental factor that can negatively affect plant growth and production. Recent studies have evaluated the effects of salinity on stomatal density, stomatal index, photosynthetic efficiency, and the leaf mesophyll of *Jatropha curcas* plants [1-4]. Exposure to salinity significantly reduced stomatal density and stomatal index, which then negatively affected photosynthetic efficiency. Altogether, the reduction in stomatal density may be one of the main causes of the decrease in photosynthetic efficiency in *J. curcas* under salt stress [1]. These results are important to understand how salinity affects plant physiology, in addition to providing more information for understanding the development of genetic improvement strategies to make the plant more tolerant to salinity.

Gas exchange is influenced by a series of factors, both environmental and internal to the plant [5]. Under water/saline stress, there is usually a lower flow of water from the roots to the leaves,

 doi:10.20944/preprints202307.0048.v1

causing them to decrease the stomatal opening for CO_2 uptake [3,6-9]. As CO_2 is the fuel for photosynthesis, lower uptake generally leads to lower photosynthetic rates. However, other factors may influence equal or greater magnitude in the modulation of photosynthesis. Under salinity, for example, as root cells absorb salt ions , their osmotic potential is reduced, which further reduces the uptake of water from the soil [10], as well as its ascent to the leaves, a process that is called hydraulic conductivity (*K*p) [11,12]. Furthermore, a simple increase in CO_2 uptake by stomata does not necessarily mean an increase in gas exchange, since CO_2 crosses several physical barriers before reaching the RuBisCo carboxylation site [13-16], a process named mesophilic conductance, analogous to stomatal conductance which is given by the change in CO_2 uptake by the stomata. However, other processes can modulate photosynthesis, such as the decrease or inactivation of enzymes in the Calvin-Benson cycle [1,9,15-18] or even the disruption of the chloroplast architecture [2,4,19-23]. The integrity and functionality of the electron transport system are crucial in the intricate process of photosynthesis, encompassing the journey from water to the generation of NADPH and ATP in the photochemical stage, and ultimately leading to the formation of triose phosphate [24]. It is imperative to maintain the integrity of chloroplasts ultrastructure to ensure an efficient utilization of captured electrons by an antenna system, primarily composed of chlorophylls. These electrons are utilized in the reduction of $NADP^+$, which transforms into its reduced form, NADPH. The resulting NADPH plays a vital role in the Calvin-Benson cycle, driving the assimilation of carbon dioxide and facilitating the synthesis of organic molecules. Thus, the maintenance of chloroplast integrity is fundamental for the overall productivity and the success of the photosynthesis [25].

Besides physiological and biochemical responses, plants are able to cope with saline conditions by making changes in the anatomical structure of leaves and roots as well as changes in some features [26]. Leaf architecture is very important to CO_2 flux in the mesophyll; therefore, the study of plant anatomy of leaf and its xylem vessels is highly interesting because with lower osmotic potential, the plant tends to reduce its water fluxes and then all metabolic events, not just simple photosynthesis. Our core hypothesis is that the reduction of vessel conductance with lower osmotic potential can reduce the translocation of trioses phosphate to cytosol, leading to an increase of starch in the chloroplast and this can disrupt the chloroplast grana structure leading to a decrease in net photosynthesis. The main goal of this study was to be demonstrated that salt stress changes the source-sink process and amylaceous structures that were formed in the chloroplast. Being heavy, these structures force the grana against the chloroplast wall, completely destroying the integrity of the thylakoids, a fact that becomes one of the main causal events of low photosynthetic rates in mesophytic plants under saline stress.

2. Results

The measured accumulated precipitation in both 2017 and 2018 was 158.1 mm and 362.8 mm, respectively (Supplementary Figure S1). Thus, we can state that the plants were in practice fully irrigated with saline water, for entire experiment, in the appropriate treatments, and based on that, the accumulated evapotranspiration was 158.3 mm and 355.5 mm, respectively in 2017 and 2018 (Supplementary Figure S1).

2.1. Cross section in leaves of J. curcas plants under salt stress

In the cross-section of *J. curcas* leaves it was observed a significant difference when comparing 1-year-old and 2-year-old *J. curcas* stressed plants (Figures 1 abd 2). For example, in the 1-year-old *J. curcas* stressed plants, the total leaf thickness (Figure 1A), the adaxial (Figure 1C) and abaxial surface thickness (Figure 1E), the thickness of the palisade parenchyma (Figure 1G), the thickness of the spongy parenchyma (Figure 2A), and palisade number (2E) was slightly (Figures 1G and 2E) and moderately (Figures 1A,C,E) increased as saline stress increased. On the other hand, all previously described features showed a median (Figure 1B) or strongly (Figures 1D,F,H, and 2B) decreased value in 2-year-old *J. curcas* stressed plants. Moreover, neither the number of palisades (Figure 2E,F), the air spaces in the mesophyll (Figure 2G,H), the area of crystals (Figure 2I,J) nor the palisade to spongy

Preprints (www.preprints.org) | NOT PEER-REVIEWED | Posted: 4 July 2023 doi:10.20944/preprints202307.0048.v1

parenchyma ratio (Figure 2C,D) changed significantly in any of the salt concentrations within the time the plants were subjected to salinity.

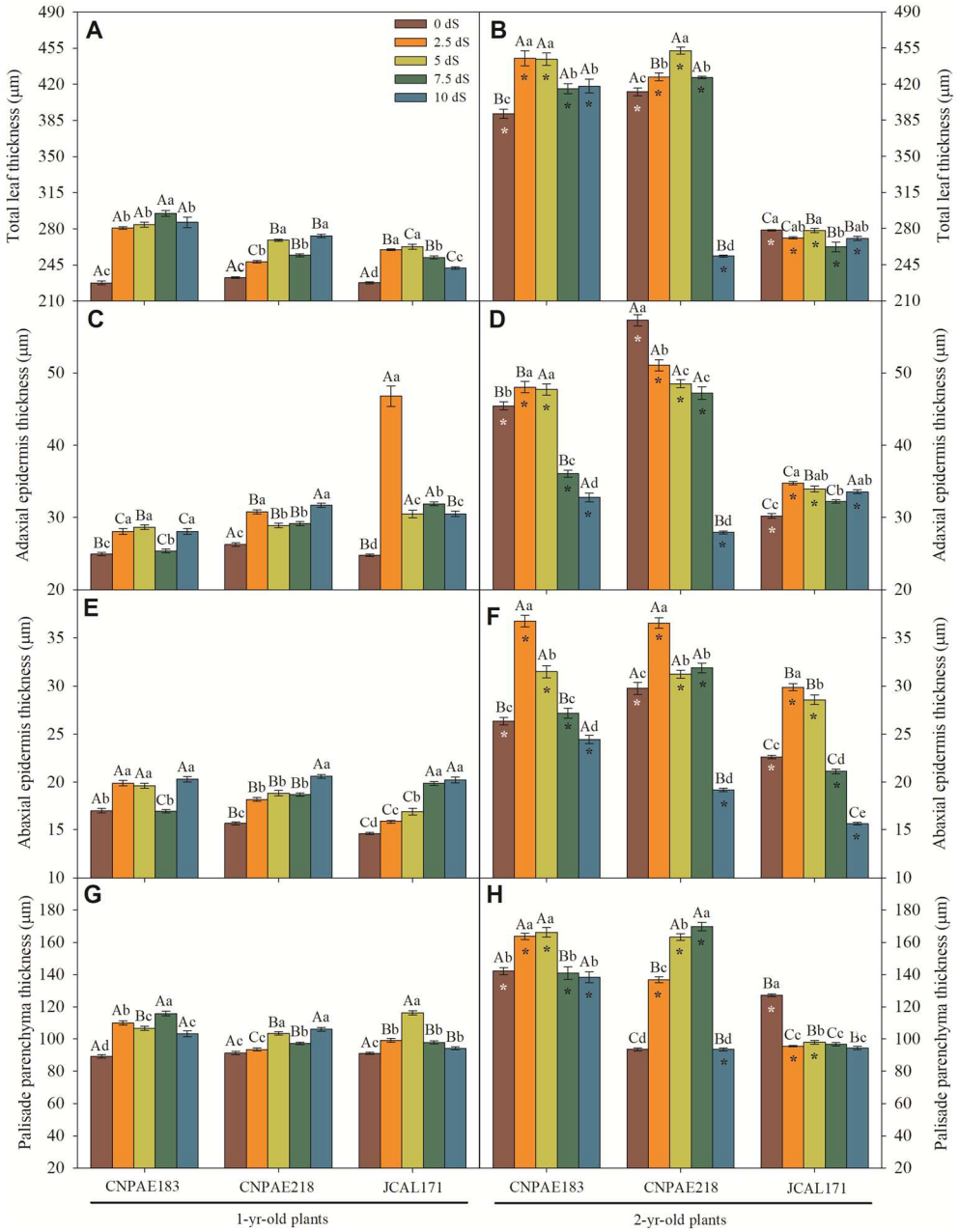

Figure 1. Total leaf thickness (A, B), adaxial epidermis thickness (C-D), abaxial epidermis thickness (E-F), and palisade parenchyma thickness (G-H) of 1-year-old (A, C, E, G) and 2-year-old (B, D, F, H) *Jatropha curcas* genotype CNPAE183, CNPAE218, and CNPAE171 subjected to irrigation water with electrical conductivities of 0 dS m^{-1}, 2.5 dS m^{-1}, 5.0 dS m^{-1}, 7.5 dS m^{-1} e 10.0 dS m^{-1}. All data are expressed as means ± SE. n = 500. Different lowercase letters denote a significance within salt concentration for each genotype; different uppercase letters denote a significance within the genotypes for the same salt concentration, and asterisks (*) denote significance within sample data (1- and 2-year-old plants).

Preprints (www.preprints.org) | NOT PEER-REVIEWED | Posted: 4 July 2023 doi:10.20944/preprints202307.0048.v1

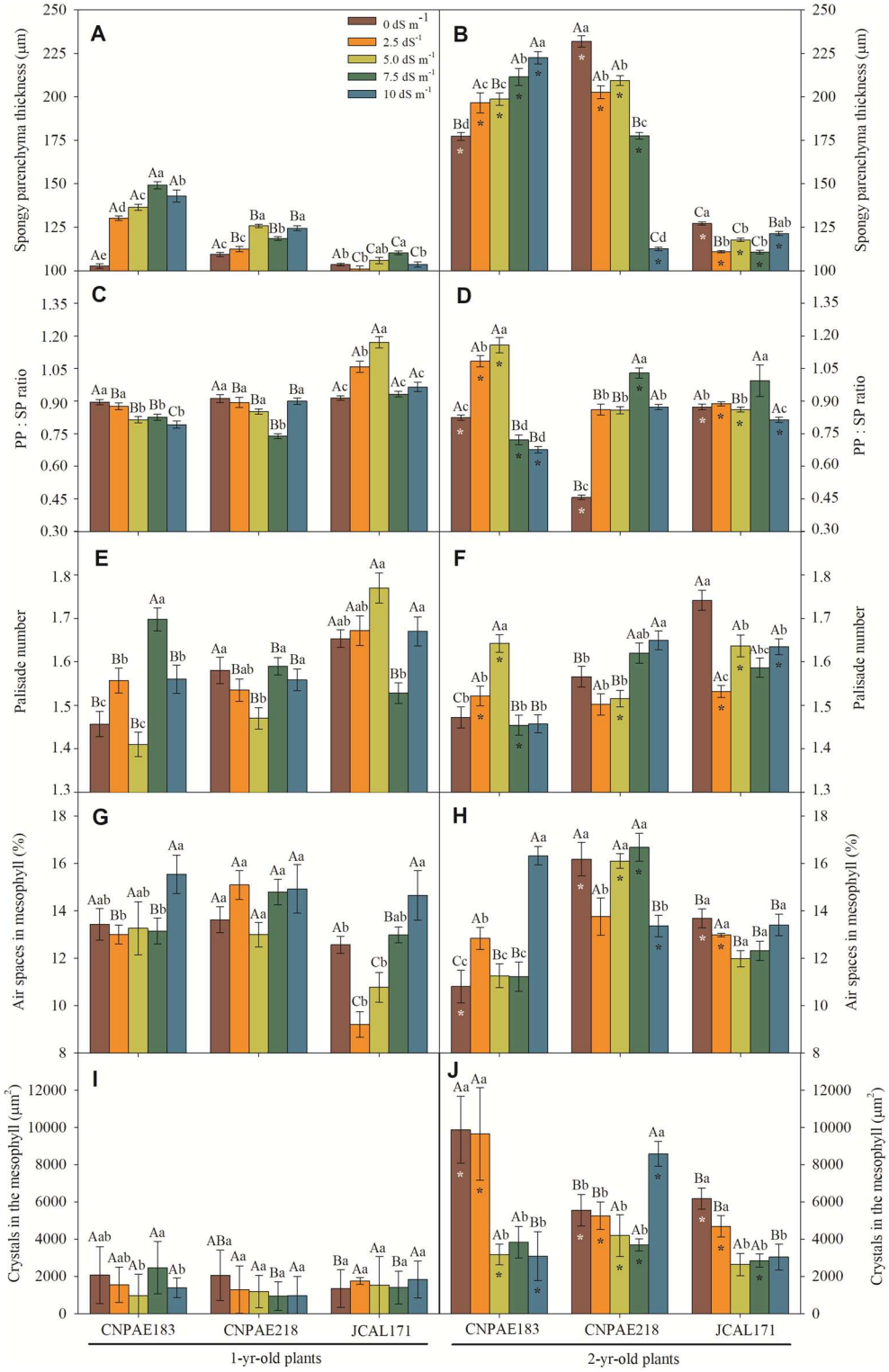

Figure 2. Spongy parenchyma thickness (A, B), palisade to spongy parenchyma (PP: PS) thickness ratio, (C, D) palisade layers on mesophyll (E, F), air spaces in mesophyll (G, H), and oxalate crystals in the mesophyll (I, J) of 1-year-old (A, C, E, G, I) and 2-year-old (B, D, F, H, J) *Jatropha curcas* genotype CNPAE183, CNPAE218, and CNPAE171 were subjected to irrigation water with electrical conductivities of 0 dS m^{-1}, 2.5 dS m^{-1}, 5.0 dS m^{-1}, 7.5 dS m^{-1} e 10.0 dS m^{-1} of electrical conductivity on irrigation water. All data are expressed as means ± SE. n = 500. Different lowercase letters denote significance within salt concentration for each genotype; uppercase letters denote significance within genotypes for the same salt concentration, and asterisks (*) denote significance within sample data (1- and 2-year-old plants).

Preprints (www.preprints.org) | NOT PEER-REVIEWED | Posted: 4 July 2023 doi:10.20944/preprints202307.0048.v1

In 1-year-old *J. curcas* stressed plants, the adaxial epidermis surface cells were on average 1.7-fold higher than those in abaxial epidermis surface. In 2-year-old *J. curcas* stressed plants, this ratio was lower but with maximum and minimum value ranging from 1.1- to 2.2-fold higher. However, on the abaxial surface, a greater presence of bistratified epidermis is observed (Figure 3A,B, E; green arrows), distinct from the adaxial surface of the epidermis. The total leaf thickness, as well as the density of the spongy mesophyll, is clearly visible (Figure 3). An increase in palisade and spongy parenchyma with saline is also evident. Similarly, the appearance of more than one palisade layer it is also common. Thus, the palisade cell number seems to increase as the salt concentration increases (Figure 2 E,F), in both 1-year-old, and 2-year-old *J. curcas* plants.

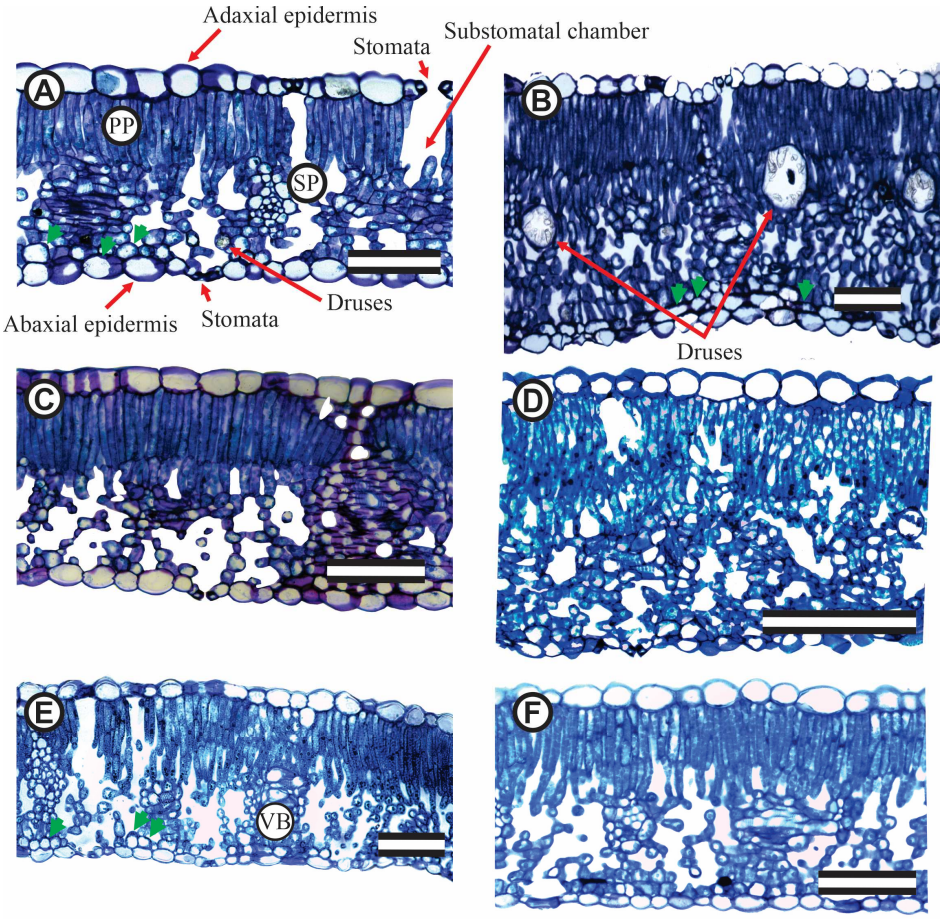

Figure 3. Light micrographs of cross-sections of the CNPAE183 (A-B), CNPAE218 (C-D), and CNPAE171 (E-F) 1-year-old *Jatropha curcas* genotypes subjected to irrigation water with electrical conductivities of 0 dS m^{-1}, (A, C, E) or 10 dS m^{-1} (B, D, F) of electrical conductivity on irrigation water. PP, palisade parenchyma. SP, spongy parenchyma. VB, vascular bundles. Green arrows represent the bistratified epidermis in the abaxial surface. Scales = 100 µm.

Similarly with mesophyll thickness, leaf blade, xylem thicknesses, the length and width of the midrib, and the vessel diameter were significantly decreased when exposed to a high level of salinity (Supplementary data file). The median value has a strong positive correlation with salinity and salt exposure time where a cross section of the leaf blade displays more evidence that salt provokes many changes in the leaf blade to cope with water stress imposed by salinity. In this sense, as salt stress increases, the lumen vessel area (Figure 4A,B), xylem area (Figure 4E,F), total xylem area (Figure 4G,H), thickness of xylem (Figure 4I,J), midrib thickness (Figure 5A,B), midrib length (Figure 4C,D), and midrib area (Figure 4E,F) decrease in a similar proportion. The correlations corroborate this pattern, since a correlation between salt concentration and xylem feature is medium to strongly and inversely correlated to the lumen vessel area (r = -0.546), xylem area (r = -0.479), total xylem area (r =

Preprints (www.preprints.org) | NOT PEER-REVIEWED | Posted: 4 July 2023 doi:10.20944/preprints202307.0048.v1

-0.724), thickness of xylem (r = -0.547), midrib thickness (r = -0.754), midrib length (r = -0.726), and midrib area (r = -0.634) (Supplementary data file).

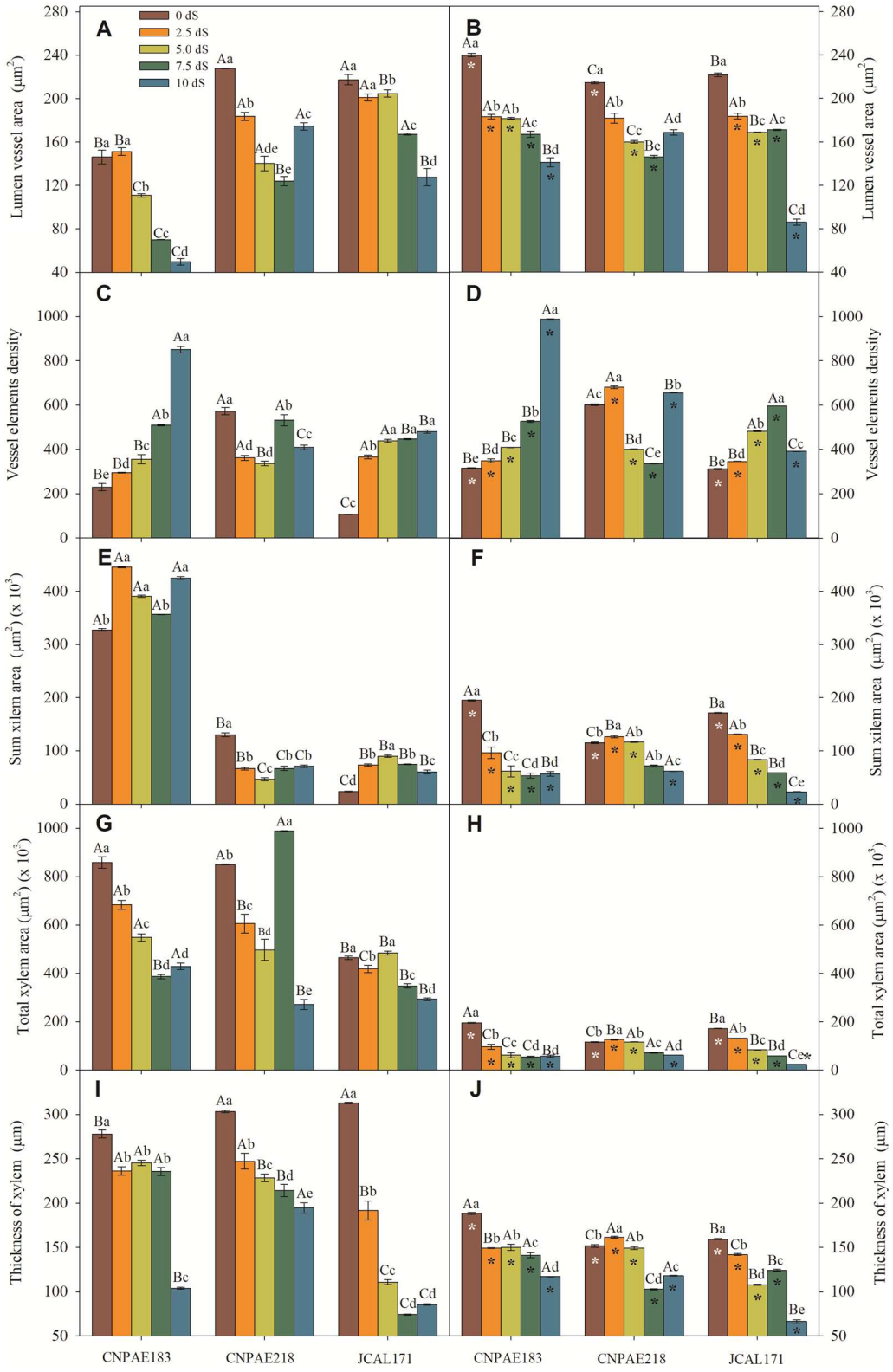

Figure 4. Lumen vessel area (A, B), vessel element density (C, D), sum xylem area (E, F), total xylem area (G, H), and thickness of xylem (I, J) measured in 1-year-old (A, C, E, G, and I) or 2-year-old plants (B, D, F, H, and J) and 3 genotypes (CNPAE183, CNPAE218, and JCAL171) of *Jatropha curcas* under control (brown), 2.5 dS m^{-1} (orange), 5.0 dS m^{-1} (yel-low), 7.5 dS m^{-1} (green), and 10.0 dS m^{-1} (blue) promoted by the addition of NaCl to the Hoagland solution. All data were measured in 100 repetitions per treatment, where in each repetition, all vessel elements were com-puted as Material and Methods.

Preprints (www.preprints.org) | NOT PEER-REVIEWED | Posted: 4 July 2023 doi:10.20944/preprints202307.0048.v1

Different lowercase letters de-note significant differences bet-ween salt concentrations within in the same genotype, and different uppercase letters denote significant differences between genotypes within the same salt concentration. Asterisks denote significant differences between 1-year-old and 2-year-old *J. curcas* plants.

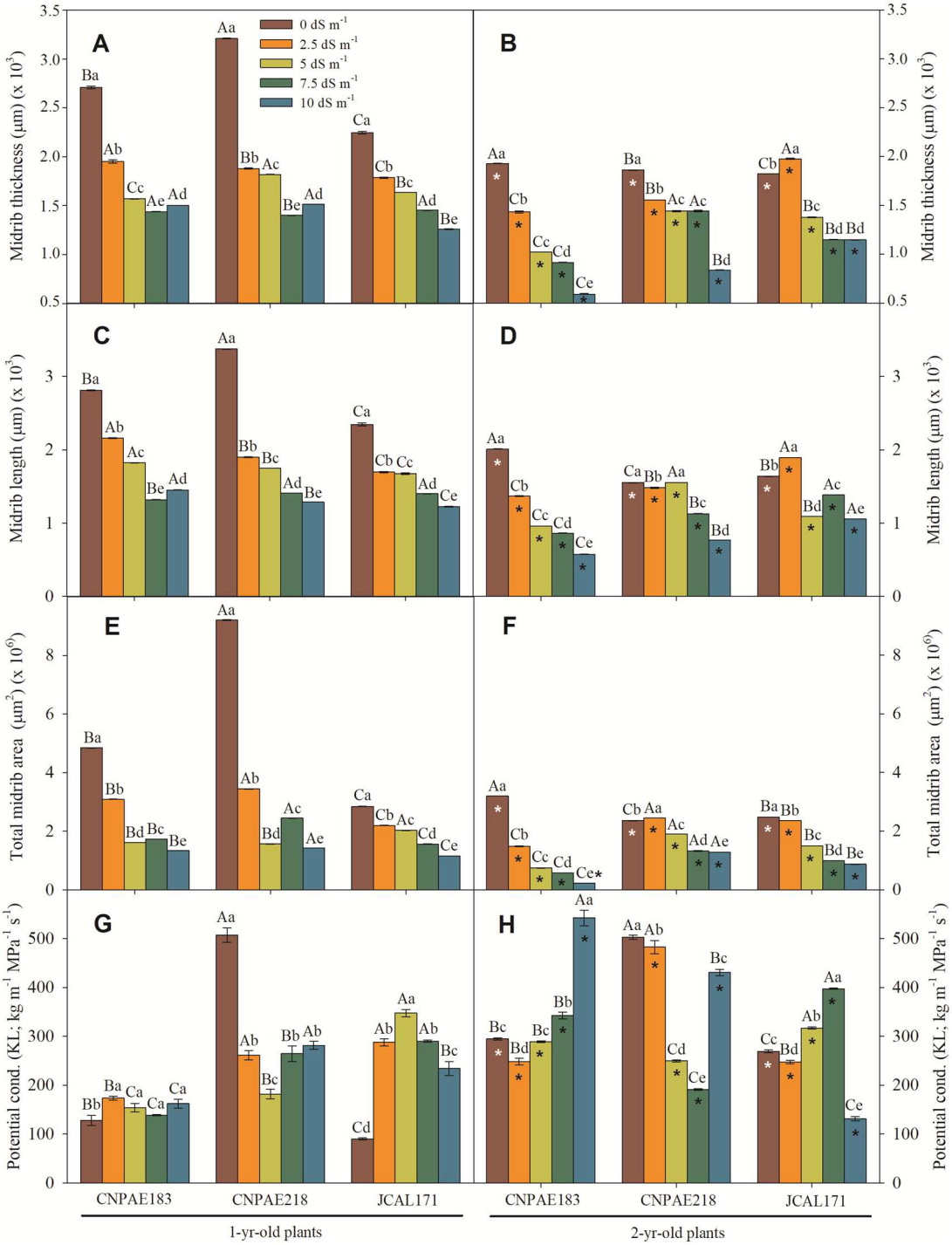

Figure 5. Midrib thickness (A, B), midrib length (C, D), total midrib area (E, F), and potential conductivity of vessels (KL; G, H) measured in 1-year-old (A, C, E, and G) or 2-year-old plants (B, D, F, and H) and 3 genotypes (CNPAE183, CNPAE218, and JCAL171) of *Jatropha curcas* under control (brown), 2.5 dS m^{-1} (orange), 5.0 dS m^{-1} (yellow), 7.5 dS m^{-1} (green), and 10.0 dS m^{-1} (blue) promoted by the addition of NaCl to a Hoagland solution. All data were measured in 100 repetitions per treatment, where in each repetition all vessel elements were computed as Material and Methods. Different lowercase letters denote significant differences between salt concentrations within the same genotype, and different uppercase letters denote significant differences between genotypes within the

 doi:10.20944/preprints202307.0048.v1

same salt concentration. Asterisks denote significant differences between 1-year-old and 2-year-old *J. curcas* plants.

Also, the lumen vessel area, xylem area, and vessel element density show a positive correlation with the potential conductivity of vessels (*K*p) measured with positive correlation like 0.460, 0.486, and 0.640, respectively, denoting more and lesser xylem cells contributing positively to the water transportation system in xylem. Similarly, the combined all xylem area (total xylem area, thickness of xylem, midrib thickness, and midrib length) shows negative (-0.201, -0.204, -0.140, -0.149) correlation with *K*p (Supplementary data file).

2.2. Scanning electron microscopy of the epidermis (SEM)

In a frontal view, both epidermises are composed of polymorphic cells, arranged with stomata densely (abaxial) or sparsely (adaxial) located. Paracytic stomata with ordinary cells of different sizes appear on both epidermis surfaces. The stomata density (SD) ranged from 169 to 424 stomata per mm^2 in the abaxial surface in 1-year-old *J. curcas* plants and from 227 to 440 stomata per mm^2 in 2-year-old *J. curcas* plants. In the adaxial epidermis surface, SD ranged from 49 to 219 stomata per mm^2 in 1-year-old *J. curcas* plants and from 33 to 234 stomata per mm^2 in 2-year-old *J. curcas* plants (Figures 6 and 7). In both surfaces of the epidermis, the SD increased as salt stress increased with CNPAE218 10 dS m^{-1} showing a higher SD as the salt stress increased. The SD ranged from 124% to 379% higher in abaxial than adaxial (Figures 6 and 7) epidermis surfaces. In respect to salinity, the CNPAE218 and CNPAE171 genotypes both increased the SD, while the in CNPAE183 SD in 10 dS m^{-1} plants were 69.3% and 82.3% lower than 0 dS m^{-1}, respectively in 1-year-old and 2-year-old *J. curcas* plants.

Similarly, abaxial ordinary cell density (OCD_{aba}) ranged from 1817 to 2819 cells mm^{-2} (Figure 8C) in 1-year-old *J. curcas* plants and from 1611 to 3009 cells mm^{-2} (Figure 8D) in 2-year-old *J. curcas* plants. Ordinary adaxial cell density (OCD_{ada}) ranged from 859 to 1689 cells mm^{-2} (Figure 8C) in 1-year-old *J. curcas* plants and from 813 to 1919 cells mm^{-2} (Figure 8D) in 2-year-old *J. curcas* plants (Figure 7C-D).

Considering only the CNPAE183 genotype, the SD of the abaxial epidermis surface decreased from 339 to 207 (-39%; 1-year-old) and from 352 to 227 (-35.5%; 2-year-old) comparing both stressed plants (10 dS m^{-1}) and its control plants. At the same time, these plants showed a reduction in the OCD_{aba} of 32.5% (1-year-old) and 17.6% (2-year-old). Thus, the stomatal index of these plants was 9% (1-year-old) and 19.4% (2-year-old) lower in salt-stressed plants. These permit us deduce that the reduction of the stomatal index (SI) in the CNPAE183 genotype was governed to a greater extent by SD than by OCD. Inversely, the genotypes CNPAE218 and CNPAE171 showed an increase in SD. In the CNPAE218 stressed plants, the SD increased by 43.8% and 26% compared from its controls, respectively for 1-year-old and 2-year-old plants. In these plants the OCD_{aba} increase in 1-year-old plants was 24.6% and in 2-year-old plants, 60.2%. Also, this tendency permits us to speculate that changes in the SI of the CNPAE218 genotype were more influenced by SD in the 1-year-old plants and by OCD in 2-year-old plants. The increase in SD of CNPAE171 (150% in 1-year-old and 80% in 2-year-old), with a corresponding increase of 58% and 40% in OCD is sufficient data to argue that in CNPAE171 the increase in SI was governed by SD more than OCD.

On the adaxial surface, the trend continues in the CNPAE183 genotype which showed a decrease in its SD by 52.3% and 66.7%, respectively in the 1-year-old and 2-year-old plants. In these plants the OCD was decreased by 43.5% and 12.8%, confirming the fact that in the CNPAE183 genotype, the SD was the force that governed the modulation in the SI. On the other hand, in genotypes CNPAE218 and CNPAE171, the SD was increased by 147% and 157% (CNPAE218; 1-year-old and 2-year-old plants) and by 113% and 79% (CNPAE171; 1-year-old and 2-year-old), while OCD was decreased by smaller magnitudes, also confirmed that in these genotypes, SD was the factor that most strongly contributed to the increase of SI in CNPAE171 plants (2-year-old) and stability in the CNPAE218 genotype. This is a confirmation that the SD is the main factor that affects the SI urge, even from the strong positive correlation between the SD and the SI on the abaxial epidermis surface (r = 0.753), while the correlation with the OCD_{aba} was 0.512. On the adaxial epidermis surface, the magnitude of

Preprints (www.preprints.org) | NOT PEER-REVIEWED | Posted: 4 July 2023 doi:10.20944/preprints202307.0048.v1

force for SI is shared in equal strength by SD and OCD_{ada}, with the correlations being negative in the order of -0.149 and -0.143 for SD and OCD_{ada}, respectively.

In a general way, the ordinary cell area (OCA), stomatal complex area, and stomatal area follow the same tendency when compared to their density. Higher density led to smaller cells, while lower density led to larger cells (Figures 8 and 9). Similarly, there were slight variations in features between times of salt. Alternatively, the differences between the abaxial and adaxial epidermis surfaces were quite distinct. For example, the OCA was 1.1- to 2.7-fold higher on the adaxial than the abaxial epidermis surfaces among 1-year-old *J. curcas* plants and between 1.6- to 2.6-fold higher among 2-year-old *J. curcas* plants. For the stomatal area, the ratio between adaxial to abaxial ranged from 1.1- to 1.4-fold in favouring the adaxial surface (Figures 8 and 9). Distinctly, the stomatal pore area was much greater when measured in the abaxial versus the adaxial epidermis surface. The ratio between abaxial and adaxial stomatal area ranged from 1.2- to 47.8-fold higher in abaxial than adaxial surface (in 1-year-old *J. curcas* plants).

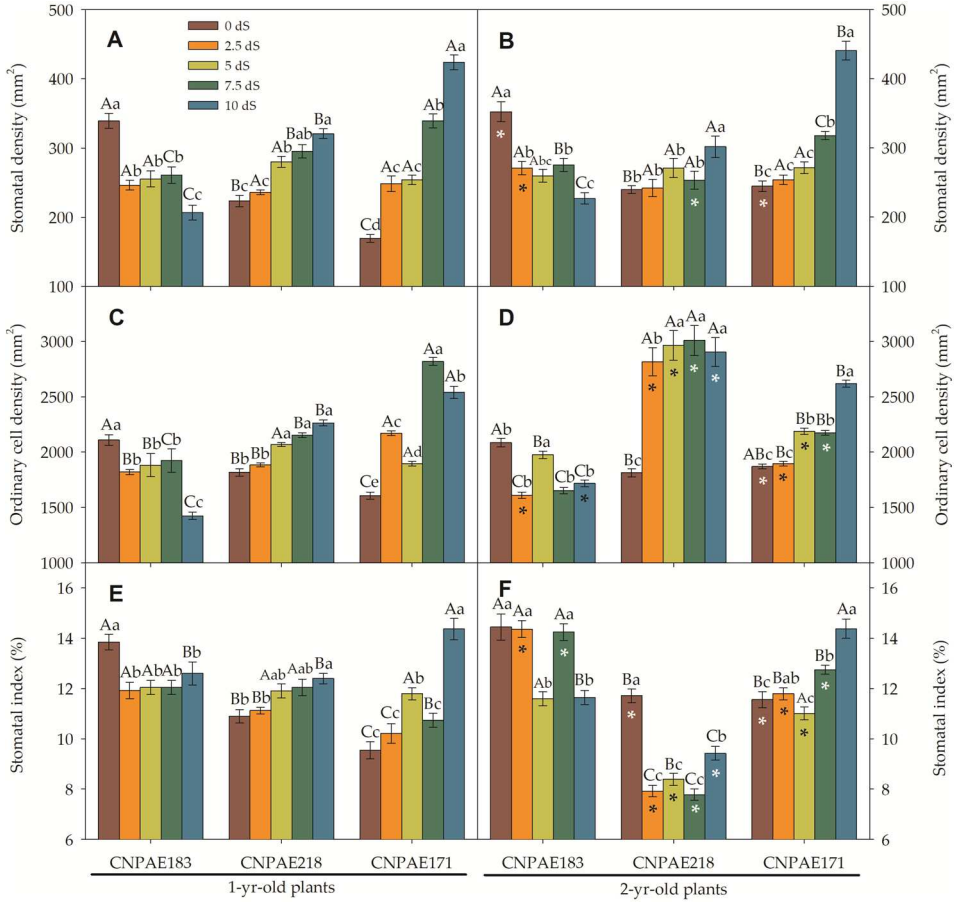

Figure 6. Stomatal density (A, B), ordinary cell density (C, D), and THE stomatal index (E, F) measured in the abaxial surface on a leaf of a 1-year-old (A, C, and E) or 2-year-old plants (B, D, and F) and 3 genotypes (CNPAE183, CNPAE218, and JCAL171) of *Jatropha curcas* under control (brown), 2.5 dS m^{-1} (orange), 5.0 dS m^{-1} (yellow), 7.5 dS m^{-1} (green), and 10.0 dS m^{-1} (blue) promoted by the addition of NaCl to a Hoagland solution. All data were measured in 20 repetitions per saline treatment, wherein each repetition all features were computed as Material and Methods. Different lowercase letters denote significant differences between salt concentrations within the same genotype, and different uppercase letters denote significant differences between genotypes within the same salt concentration. Asterisks denote significant differences between 1-year-old and 2-year-old *J. curcas* plants.

Preprints (www.preprints.org) | NOT PEER-REVIEWED | Posted: 4 July 2023 doi:10.20944/preprints202307.0048.v1

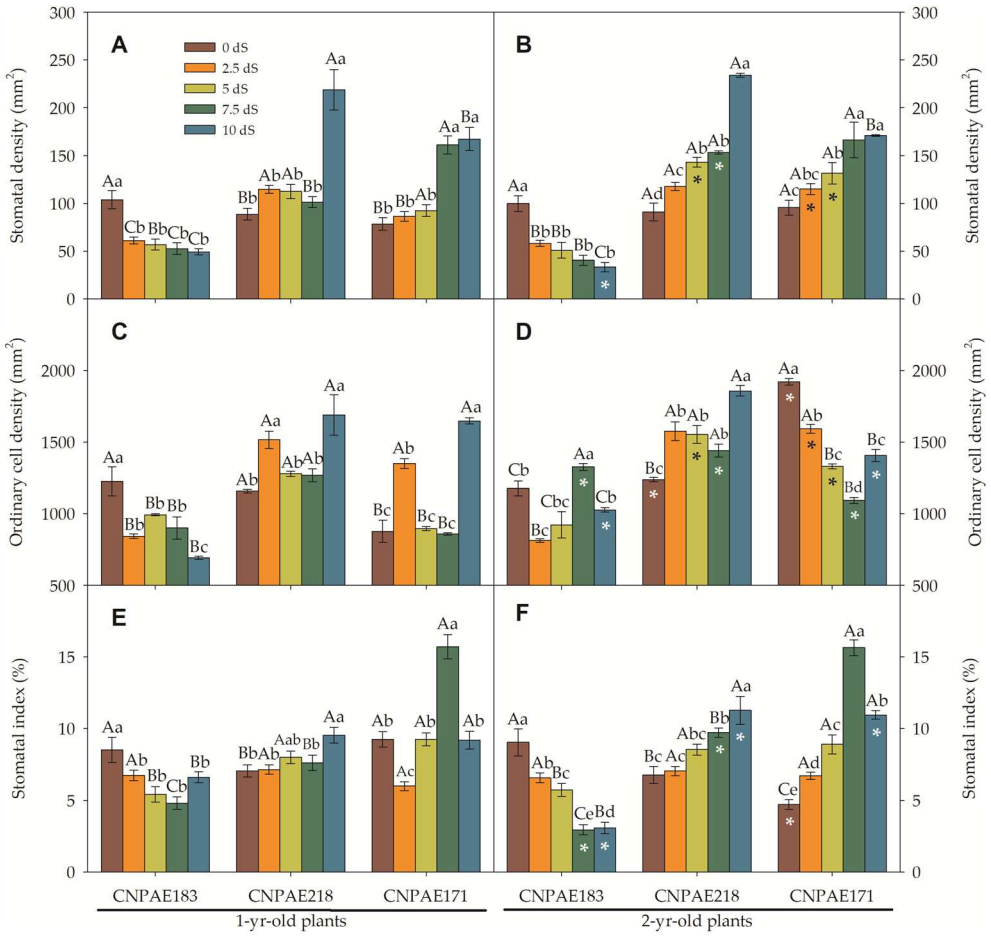

Figure 7. Stomatal density (A, B), ordinary cell density (C, D), and stomatal index (E, F) measured in leaf adaxial surfaces of leaves from a 1-year-old (A, C, and E) or 2-year-old plant (B, D, and F) and 3 genotypes (CNPAE183, CNPAE218, and JCAL171) of *Jatropha curcas* under control condition (brown), 2.5 dS m^{-1} (orange), 5.0 dS m^{-1} (yellow), 7.5 dS m^{-1} (green), and 10.0 dS m^{-1} (blue) promoted by the addition of NaCl to a Hoagland solution. All data were measured in 20 repetitions per saline treatment, where in each repetition all features were computed as Material and Methods. Different lowercase letters denote significant differences between salt concentrations within the same genotype, and different uppercase letters denote significant differences between genotypes within the same salt concentration. Asterisks denote significant differences between 1-year-old and 2-year-old *J. curcas* plants.

Figure 10 shows the arrangement of epidermal cells, both on the adaxial (Figure10A) and abaxial (Figure 10B) epidermis surface. Completely closed or all open stomata are rarely observed in the captured images (Figure 10C). As for the stomata, they may have subsidiary cells (Figure 10D) with or without visible striations (Figure 10E) oriented in an orthogonal plane with the stomata. The abaxial epidermis is very hairy (Figure 10F,G) with brightly coloured and unicellular epidermal hairs originating from epithelial cells. It seems reasonable to assume that these hairs favour stomatal opening by producing a microclimate close to the stomata or even providing another barrier to water loss, making water loss difficult, even microphotographs if no previous procedure is taken.

Preprints (www.preprints.org) | NOT PEER-REVIEWED | Posted: 4 July 2023 doi:10.20944/preprints202307.0048.v1

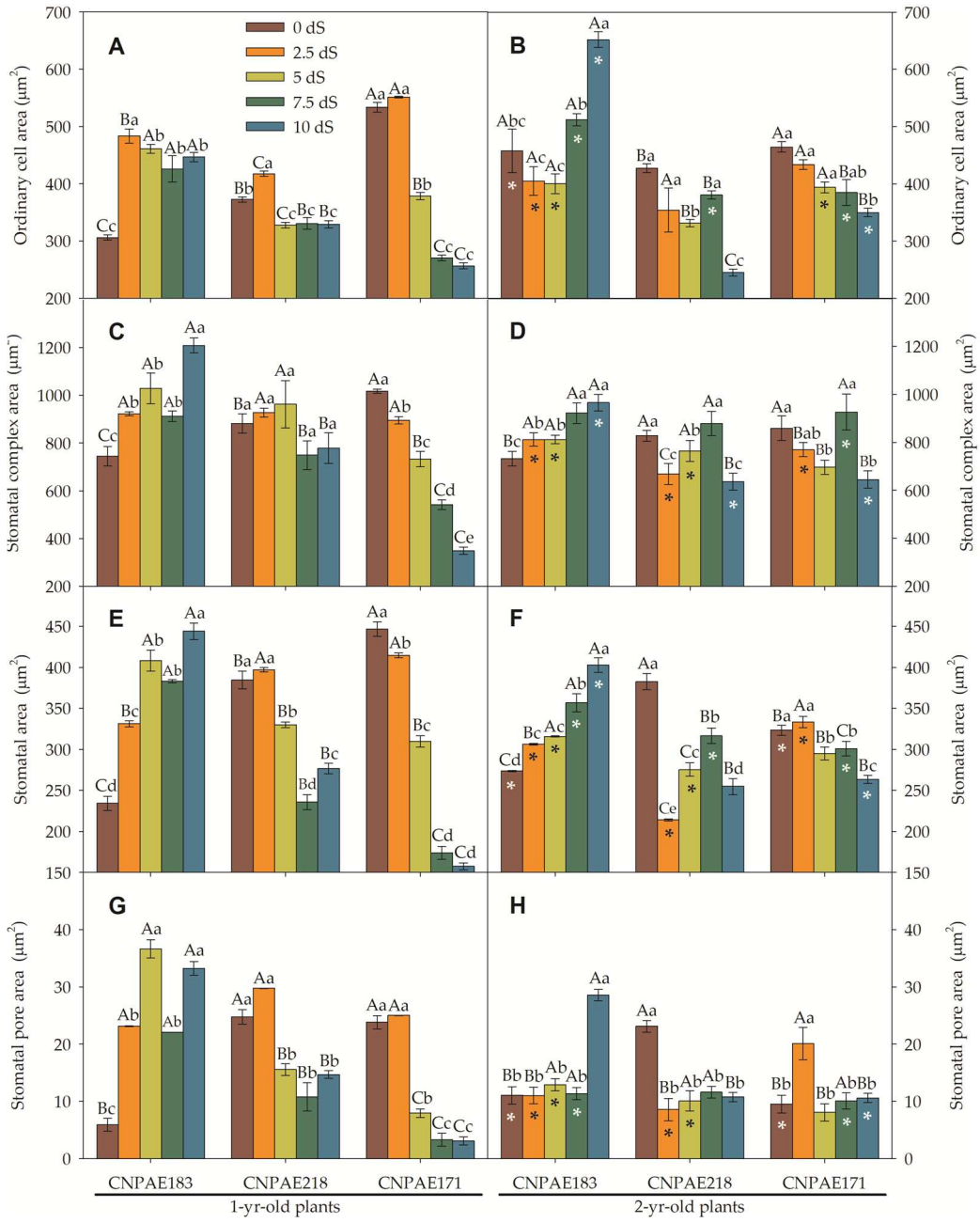

Figure 8. Ordinary cell area (A, B), stomatal complex area (C, D), stomatal area (E, F), and stomatal pore area (G, H) measured in the abaxial surfaces of leaves from 1-year-old (A, C, E, and G) or 2-year-old plants (B, D, F, and H) and 3 genotypes (CNPAE183, CNPAE218, and JCAL171) of *Jatropha curcas* under control condition (brown), 2.5 dS m^{-1} (orange), 5.0 dS m^{-1} (yellow), 7.5 dS m^{-1} (green), and 10.0 dS m^{-1} (blue) promoted by the addition of NaCl to a Hoagland solution. All data were measured in 500 (A, B) and 30 (C-H) repetitions per treatment, wherein each repetition, all features were computed as Material and Methods. Different lowercase letters denote significant differences between salt concentration within the same genotype, and different uppercase letters denote significant differences between genotypes within the same salt concentration. Asterisks denote significant differences between 1-year-old and 2-year-old *J. curcas* plants.

Preprints (www.preprints.org) | NOT PEER-REVIEWED | Posted: 4 July 2023 doi:10.20944/preprints202307.0048.v1

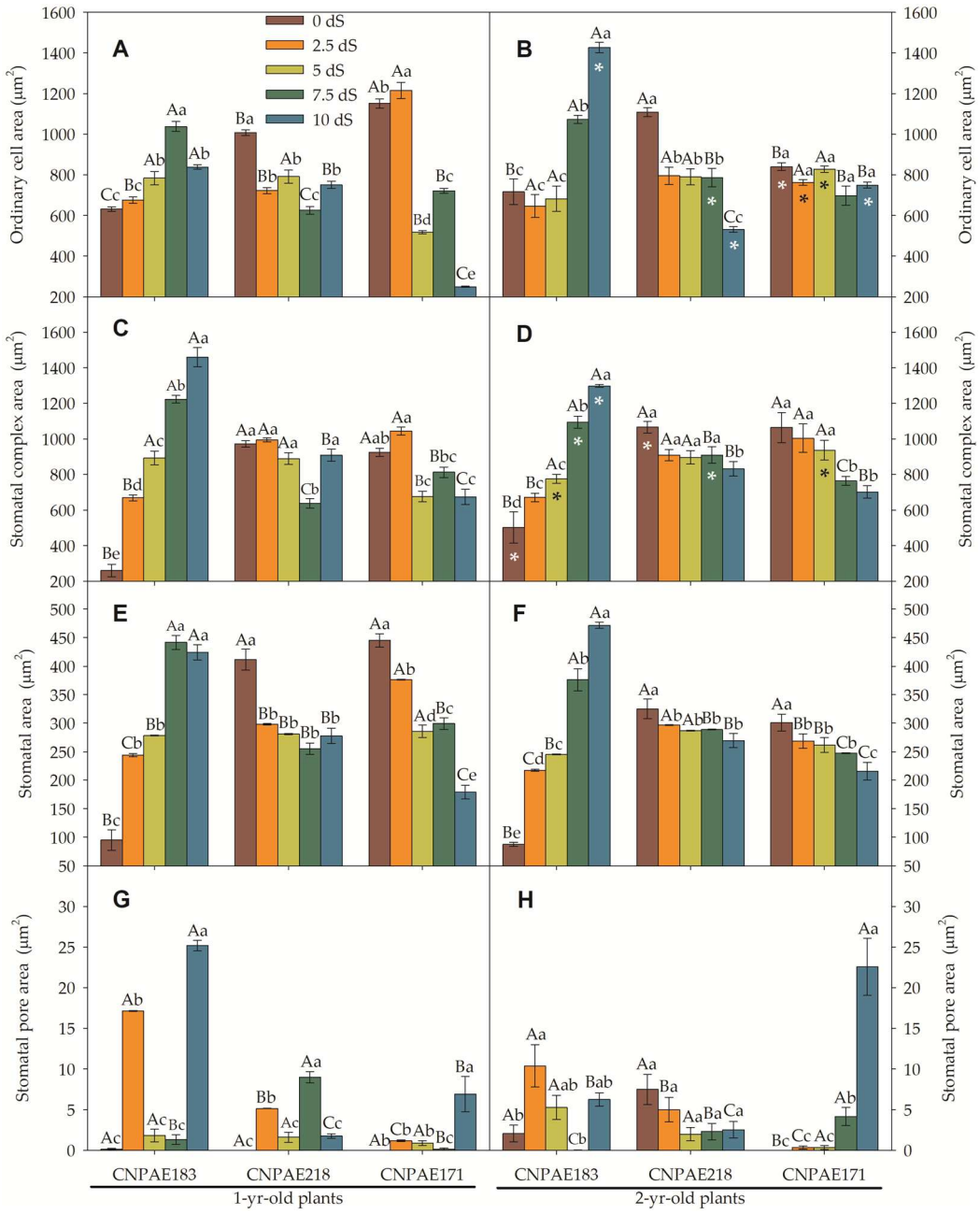

Figure 9. Ordinary cell area (A, B), stomatal complex area (C, D), stomatal area (E, F), and stomatal pore area (G, H) measured in the adaxial surface of leaves from of 1-year-old (A, C, E, and G) or 2-year-old plants (B, D, F, and H) and 3 genotypes (CNPAE183, CNPAE218, and JCAL171) of *Jatropha curcas* under control conditions (brown), 2.5 dS m^{-1} (orange), 5.0 dS m^{-1} (yellow), 7.5 dS m^{-1} (green), and 10.0 dS m^{-1} (blue) promoted by the addition of NaCl to a Hoagland solution. All data were measured in 500 (A, B) and 30 (C-H) repetitions per treatment, wherein each repetition all features were computed as Material and Methods. Different lowercase letters denote significant differences between salt concentration within the same genotype, and different uppercase letters denote significant differences between genotypes within the same salt concentration. Asterisks denote significant differences between 1-year-old and 2-year-old *J. curcas* plants.

Preprints (www.preprints.org) | NOT PEER-REVIEWED | Posted: 4 July 2023 doi:10.20944/preprints202307.0048.v1

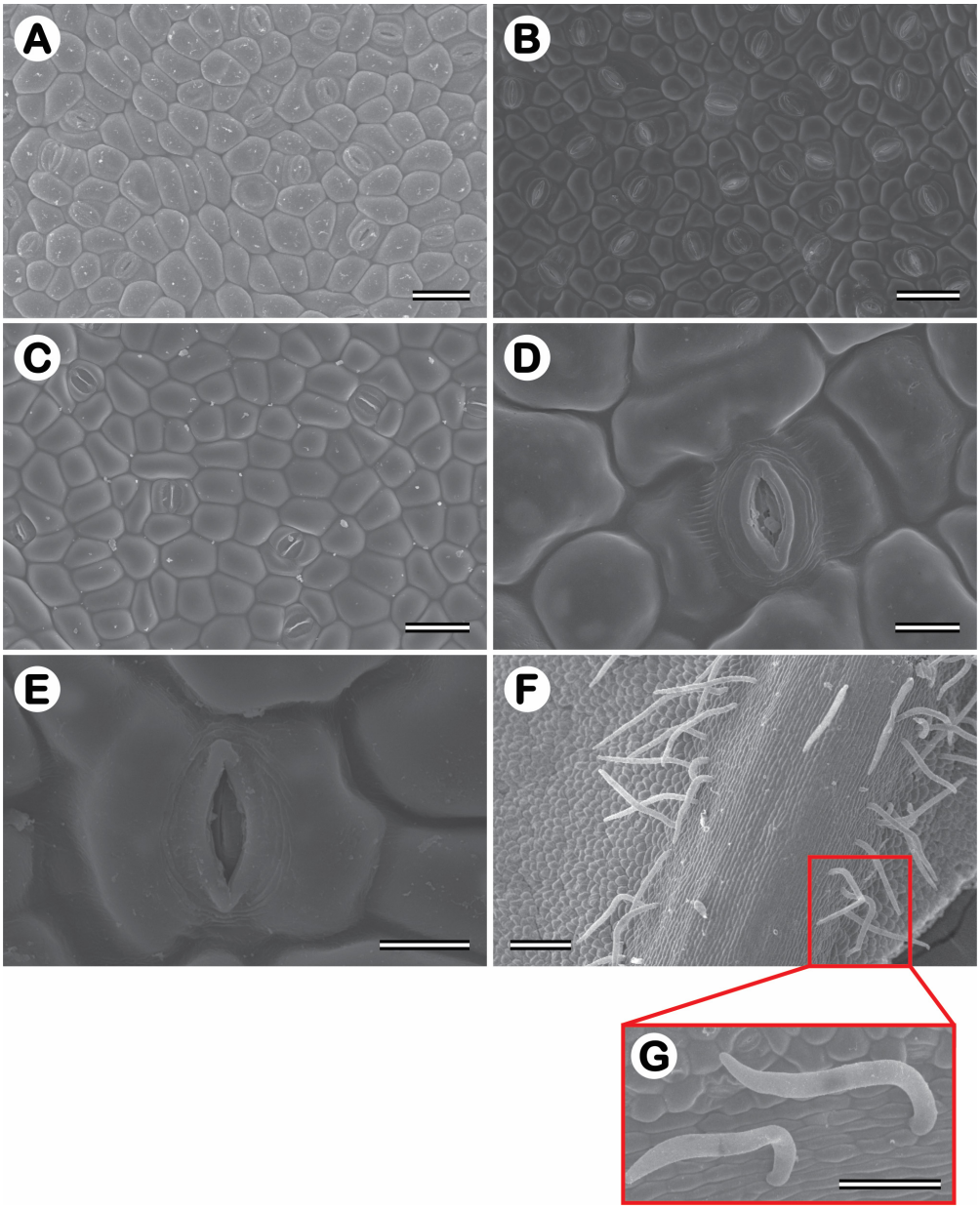

Figure 10. Scanning electron microscopy (SEM) showing abaxial (A-B) and adaxial (C) epidermis surfaces with fully open, partially-opened, and closed stomata. In D and E display stomata with the highest magnitude which exhibit both striated (D) and non-striated open stomata, both on the abaxial epidermis surface. In F, a low magnitude of abaxial epidermis surfaces displaying a very hairy and reflective abaxial epidermis which is detailed as shown in G. Scales: A-C, 50 µm; D-E, 10 µm, and F-G, 100 µm. All images were captured in 2-year-old *Jatropha curcas* plants under 0 dS m^{-1} (A-B, D-E) and 10 dS m^{-1} (C) after SEM preparation.

2.3. Transmission electron microscopy of chloroplasts (TEM)

In this study, only the control and 10 dS m^{-1} treatments were evaluated at three different points in times (Figure 11), before stress (Figure 12), in 1-year-old plants (Figure 13), and in 2-year-old plants (Figure 14). NaCl affected the ultrastructure of the chloroplast (Figure 2). In the leaf fragments visualized before stress, very well-formed chloroplasts are observed in a regular ellipsoidal-shaped arrangement with rare plastoglobules and some small, formed starch granules, was observed only in the images of the CNPAE171 genotype. In non-stressed plants, a well-formed structure of thylakoid granas and thylakoidal and stromal lamellas were described in tune with each other was verified; while chloroplasts from salinity-impacted cells swollen thylakoids were very frequent, especially in

Preprints (www.preprints.org) | NOT PEER-REVIEWED | Posted: 4 July 2023 doi:10.20944/preprints202307.0048.v1

the CNPAE218 and CNPAE171 genotypes. The disorganization of thylakoid membranes within chloroplasts is often accompanied by the disappearance of grana stacking (Figures 12–14), resulting in significant alterations to the photosynthetic machinery. This disruption can lead to impaired light harvesting and electron transport processes, ultimately affecting the overall efficiency of net photosynthesis [1].

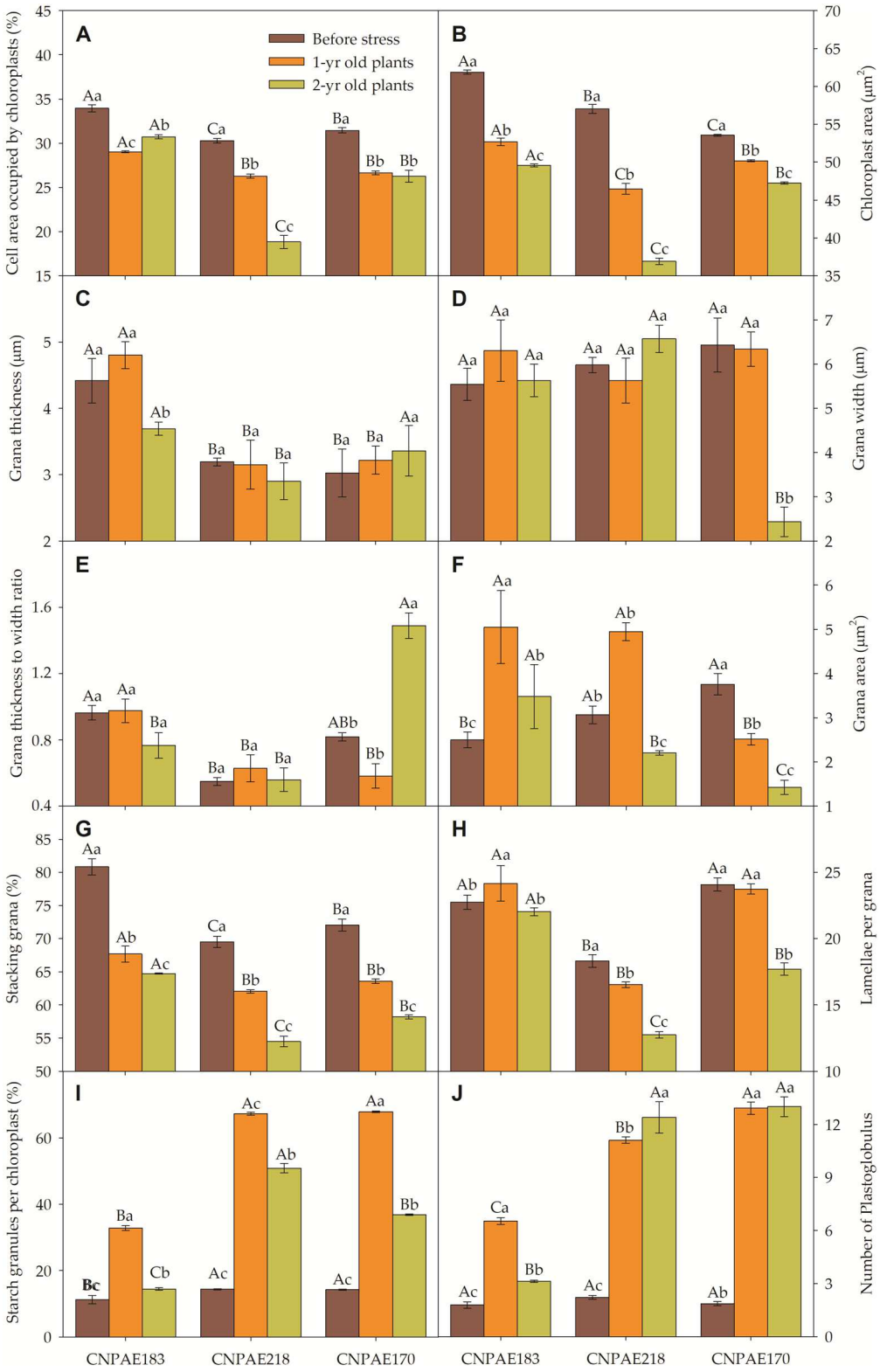

Figure 11. Chloroplast features measured in a 5 mm² ultra-thin of 1-yr old, 2-yr old, plus control of *Jatropha curcas* plants under 10.0 dS m⁻¹ promoted by NaCl addiction on Hoagland solution. All measurements data were taken from 25 ultra-thin cuts (5 mm²) from at least 3 replicates as described

Preprints (www.preprints.org) | NOT PEER-REVIEWED | Posted: 4 July 2023 doi:10.20944/preprints202307.0048.v1

in Material and Methods. Different lowercase letters denote significant differences between salt concentration within the same genotype, and different capital letters denote significant differences between genotypes within the same salt concentration.

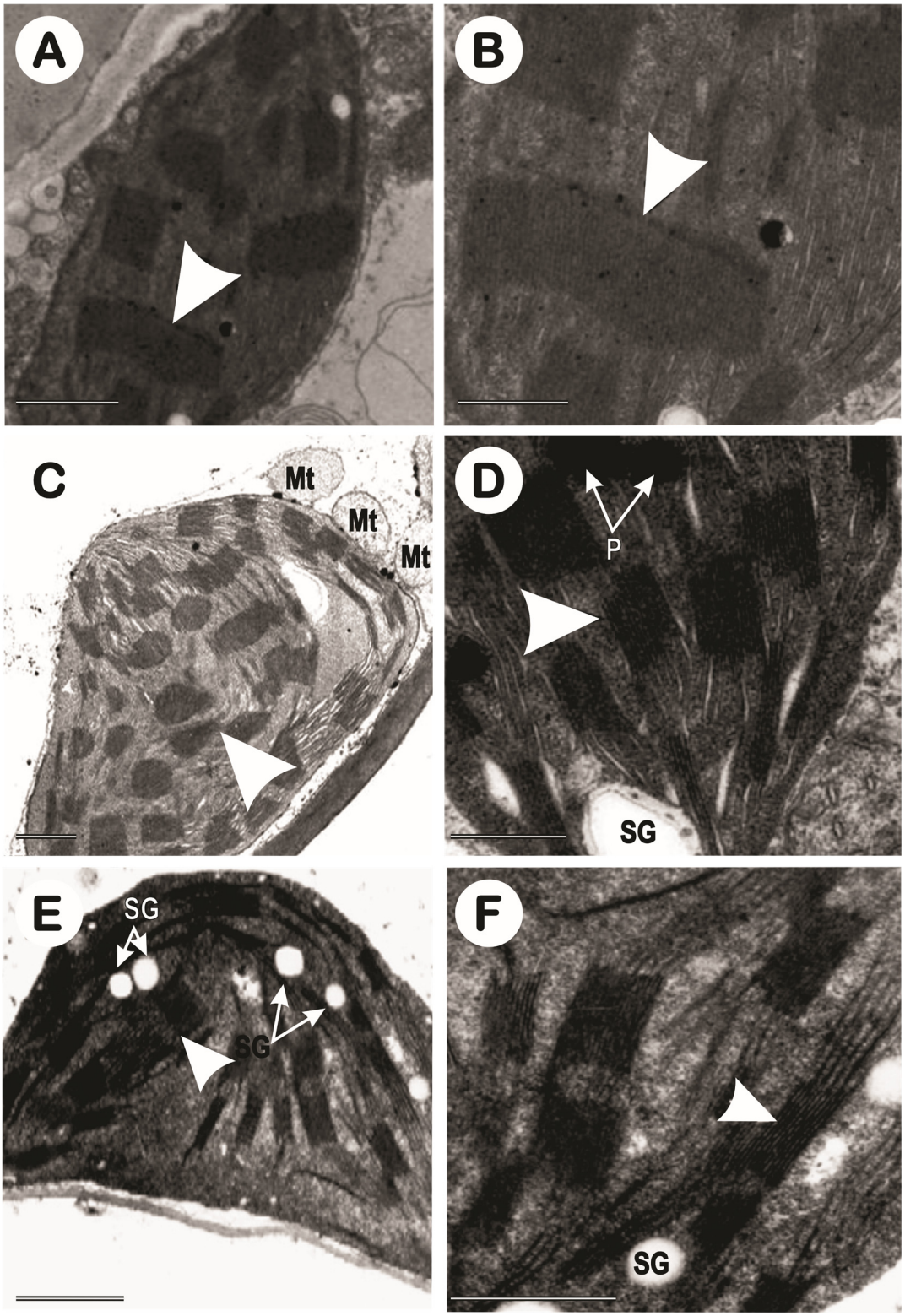

Figure 12. TEM showing regular ellipsoidal-shaped chloroplasts of CNPAE183 (A, B), CNPAE171 (C, D), and CNPAE218 (E, F) *Jatropha curcas* genotypes before salt stress. All images show granal lamellae (large white arrows), plastoglobulus (P), and starch grains (SG). A, C, and E show an overview of chloroplasts while B, D, and F display an overview of granum and stroma lamellae. Also in C, mitochondria (Mt) are visible. Scales: A, C and E, 1 µm, and B, D, and F, 500 nm.

Preprints (www.preprints.org) | NOT PEER-REVIEWED | Posted: 4 July 2023 doi:10.20944/preprints202307.0048.v1

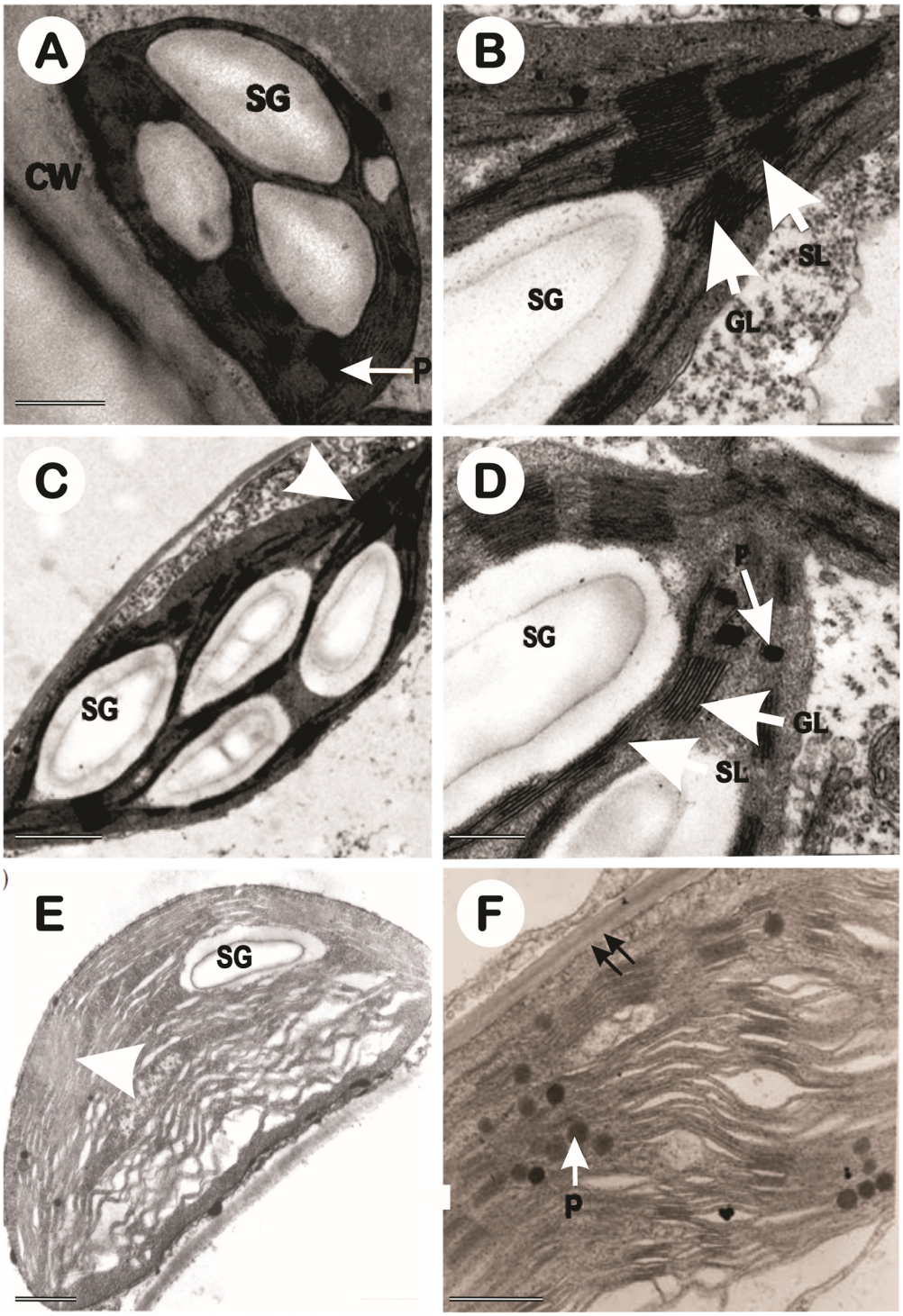

Figure 13. Transmission electron microscopy (TEM) showing regular ellipsoidal-shaped chloroplasts of CNPAE183 (A, B), CNPAE171 (C, D), and CNPAE218 (E, F) in 1-year-old *Jatropha curcas* genotypes under to 10 dS m^{-1} EC. All images show large starch grains (SG), granal lamellae (big white arrows; GL), plastoglobulus (P), and stroma lamellae (SL). A, C, and E show an overview of chloroplasts and B, D, and F display an overview of granum and stroma lamellae. In A, the cell walls (CW) are visible; and in F, a disruption of the outer envelope (black arrows) is highlighted. Scales: A, C and E, 1 µm, and B, D, and F, 500 nm.

Preprints (www.preprints.org) | NOT PEER-REVIEWED | Posted: 4 July 2023 doi:10.20944/preprints202307.0048.v1

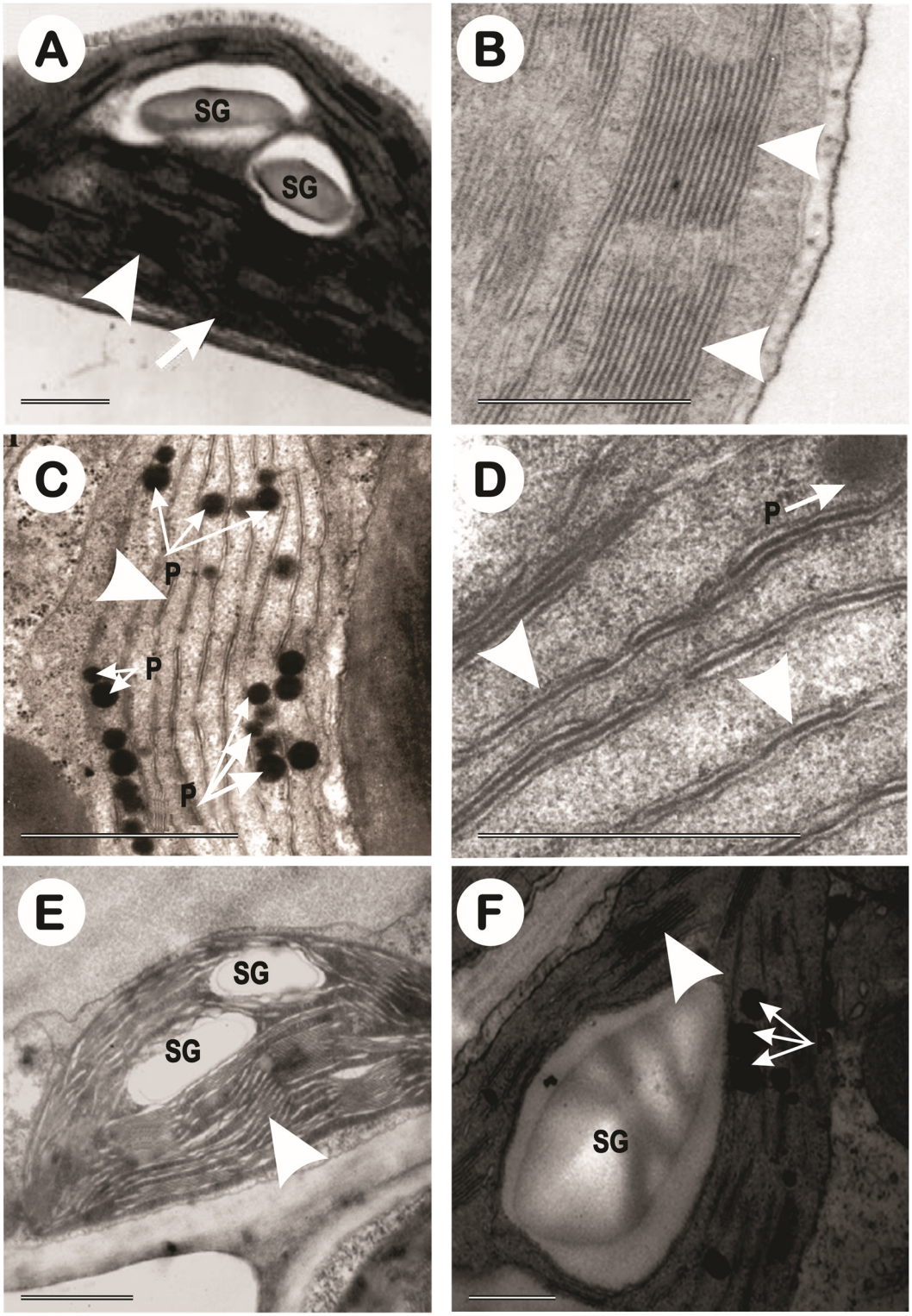

Figure 14. Transmission electron microscopy (TEM) showing regular ellipsoidal-shaped chloroplasts of CNPAE183 (A, B), CNPAE171 (C, D), and CNPAE218 (E, F) 2-year-old *Jatropha curcas* genotype plants under to 10 dS m^{-1} EC. All images show big starch grains (SG), granal lamellae (large white arrows; GL), plastoglobulus (P), and stroma lamellae. A, C, and E show an overview of chloroplast and B, D, and F displays an overview of granum and stroma lamellae. In C, numerous plastoglobules are visible. In D, and F a disruption of thylakoids caused by large starch grains is highlighted, as a contrast against A which displays intact grana and stroma lamellae. Scales: A, C and E, 1 µm, and B, D, and F, 500 nm.

Preprints (www.preprints.org) | NOT PEER-REVIEWED | Posted: 4 July 2023 doi:10.20944/preprints202307.0048.v1

The density of chloroplast per parenchyma cell was 34, 30, and 31 chloroplasts per cell, respectively in genotypes CNPAE183, CNPAE218, and CNPAE171, in plants evaluated before stress. However, this value dropped to 29 (-14.5%), 26 (-13.2%), and 27 (-15.3%) in the 1-year-old plants and to 31 (-9.5%), 19 (-37.8%) and 26 (-26%) in 2-year-old stressed *J. curcas* plants, respectively in CNPAE183, CNPAE218, and CNPAE171 (Figure 11A). While chloroplast density per cell had a slight drop, the chloroplast size (Figure 11B) was more strongly affected in the salt-stressed *J. curcas* plants, both in 1-year-old or in 2-year-old salt-stressed *J. curcas* plants. The size of chloroplasts before stress was 62 µm, 57 µm, and 54 µm, respectively in CNPAE183, CNPAE218, and CNPAE171 and dropped to 53 µm (-14.9%), 46 µm (-18.5%), and 50 µm (-6.3%) in the 1-year-old plants and to 50 µm (-19.9%), 37 µm (-35.3%), and 47 µm (-11.8%) in the 2-year-old plants. Also, chloroplast density showed a significant decrease as salinity increased. This perception must be evaluated using two methods: the cell area occupied by chloroplast (Figure 11A) and chloroplast area (Figure 11B) or by the negative correlation between cell area occupied by chloroplasts x salt exposure (r = -0.335), cell area occupied by chloroplasts x salt concentration (r = -0.169) or chloroplast area x salt concentration (r = -0.762) (Supplementary data file).

The grana thickness of the CNPAE183 genotype was lightly reduced by 16.4% in the 2-year-old plants (Figure 11C). However, the grana thickness of the CNPAE183 genotypes was on average 42%, 51%, and 18% thicker than the average grana of the CNPAE218 and CNPAE171 genotypes at times 0, 12, and 24 months (Figure 11). The grana width (Figure 11D) except the CNPAE171 genotype 2-year-old plants, which showed no significant difference in any other treatment or genotype; was a factor that was reflected in the thickness to width grana ratio (Figure 11E).

The chloroplast area occupied by grana lamellae (above 5 lamellae per grana) (Figure 11F) was significantly increased in the CNPAE183 and CNPAE218 genotypes in the 1-year-old plants even though in the 2-year-old plants the percentage had significantly decreased in all the genotypes. The percentage of grana lamellae among granal and stromal lamellae dropped from 80.9% to 67.7%, and 64.7% (genotype CNPAE183 in the 0 to 1-year-old, and the 2-year-old plants), from 69.5 % to 62.1% and 54.5 (CNPAE218 genotype in the 0 to 1-year-old plants and 2-year-old plants), and from 72% to 63.6% and 58.2% (CNPAE171 genotype 0 to 1-year-old, and 2-year-old plants). This greater or lesser stacking of the lamellae can also be verified in the lamellae by grana, where the genotype CNPAE183 did not change its percentage while in CNPAE218 and CNPAE171 they showed a sudden drop.

Both, the presence of starch grain and plastoglobulus increase as the salt stress increases. However, this increase was genotype-dependent. While in CNPAE183, the relative starch granules per chloroplast increased from 11.2% to 32.8% (+193% in 1-year-old) and 14.4% (+29% in 2-year-old), the increase in CNPAE218 was 14.4% to 67.3 (+368% in 1-year-old) and 50.9 (+254% in 2-year-old), and CNPAE171 increased from 14.2% to 67.9% (+377% in 1-year-old), and 36.9% (+159% in 2-year-old). The plastoglobulus density increased from 1.8 to 6.5 (+267% in 1-year-old) and 3.1 (+76% in 2-year-old) for CNPAE183; from 2.2 to 11.1 (+403% in 1-year-old) and 12.4 (+461% in 2-year-old) for CNPAE218; and from 1.9 to 12.9 (+595% in 1-year-old) and 13 (+600% in 2-year-old) for CNPAE171.

Morphologically, in accordance with the plants lifetime, the previously healthy chloroplasts, with well-formed and easily identified structures, became primarily starch-storing chloroplasts, which, due to their density, gradually squeezed the granal lamellae against the chloroplast walls, causing the walls to rupture almost completely (Figures 13 and 14) and caused the formation of many plastoglobules (Figures 13 and 14).

It was also verified that the chloroplasts acquired a readaptation-like capability with regards to the salinity; a fact that was very clear in the 2-year-old plants of the CNPAE218 genotype. This genotype restarted a very slow process of reorganizing the granal lamellae (Figure 14D), even if still very incipient, and showed a significant formation of plastoglobules (Figure 14C). The CNPAE171 genotype, which in the 1-year-old plants, did not show a clear formation of granal lamellae, resumed the formation of granal lamellae after the acclimatization of the 2-year-old plants. (Figure 14E,F).

2.4. Principal component analysis (PCA)

 doi:10.20944/preprints202307.0048.v1

The PCA is composed of PC1 + PC2, totalling 0.732, *i.e.* all possible variation could be represented by this PCA with 73.2% of possibilities. With 42% similarity, the PCA shows the formation of 4 groups including all treatments. The 1st group is a cluster of 6 combinations of genotype and salt concentration. The 2nd group is a cluster of 3 treatments of CNPAE183 (0, 2.5, and 5 dS m^{-1}) plus CNPAE171 5 dS m^{-1}. The 3rd group is a cluster of 4 combinations of genotype and salt concentration, and finally, the 4th group contains a singular analysis composed of only one treatment (CNPAE171 2.5 dS m^{-1}) (Figure 15A,B). Figure 15C shows that the featured grana area, grana width, grana stacking, grana thickness, chloroplast area, lamellae per grana, starch, and plastoglobulus are in the same PCA slot, showing that there are shared similarities. However, to understand the relationship between them, grana stacking will be isolated, as it will be better presented in Section 3 (discussion), it is one of the best indicators for analyzing the integrity of chloroplasts. So, the correlation between grana stacking and grana area, and grana width, return median and positive correlation is measured as 0.234, and 0.312, respectively. Other correlations with grana stacking were strong as evidenced by grana thickness (r = 0.864), chloroplast area (r = 0.765), and lamellae per grana (r = 0.776). Two other correlations between grana stacking and starch (r = -0.748) and plastoglobulus (r= -0.949) were strongest but negatively correlated. Lamellae per grana and plastoglobulus also have a strong negative (r = -0.866) correlation. Thus, we can argue that the integrity of chloroplasts is promoted by the size of the starch grains, the size of the chloroplasts and the average number of lamellae per grana. The presence of starch grains, due to their high density, presses the grains against the chloroplast wall (Figures 13A,C and 14F) destroying the walls and generating a large concentration of plastoglobules, since the correlation between starch grains and plastoglobules was rather high (r = 0.812).

The heat map analysis (Supplementary Figure S2) reviews all features analyzed in this study. With this point of view, it is easy to perceive that as salt stress increase, there is an increase in the number of xylem cells for all genotypes and salt conditions. There is also a decrease in the thickness of xylem cells, midrib thickness, midrib length, and midrib area as salt stress increases. Additionally, the salt stress increases the stomatal pore area on the abaxial epidermis surfaces on CNPAE183 and CNPAE171, while on CNPAE218, it decreases. The same pattern was observed on the stomatal complex area and stomatal area, both on adaxial epidermis surfaces. However, in 2-year-old plants both features strongly increase for all genotypes and salt stresses, mainly in CNPAE218 and CNPAE171 genotypes. It's clear that the starch granules and plastoglobulus significantly increase in both 1-year-old and 2-year-old J. curcas plants under 10 dS m^{-1} of electric conductivity.

3. Discussion

Salt-stressed *J. curcas* plants produce smaller leaves [1,2,9,27]. Smaller leaves show closely packed epidermal cells and other tissues, causing a higher stomata density, an ordinary leaf area density and higher xylem cells per area. As previously reported for cotton [28], the abaxial surface of the epidermis may be more active during salt stress than the adaxial surface. This finding is a result of the increase in the abaxial/adaxial ratio and from the fact that only the abaxial surfaces have reflective trichomes described, situated close to the veins (Figure 10F,G). With an increased salinity, smaller leaves have higher convection coefficients and a lower resistance to heat transfer through leaf boundary layers than larger leaves, and leaf size may change to optimize leaf temperature [29,30]. Larger leaves may be intrinsically vulnerable to drought-induced embolism due to the lower vein length and larger xylem conduit diameters [31,32].

Preprints (www.preprints.org) | NOT PEER-REVIEWED | Posted: 4 July 2023 doi:10.20944/preprints202307.0048.v1

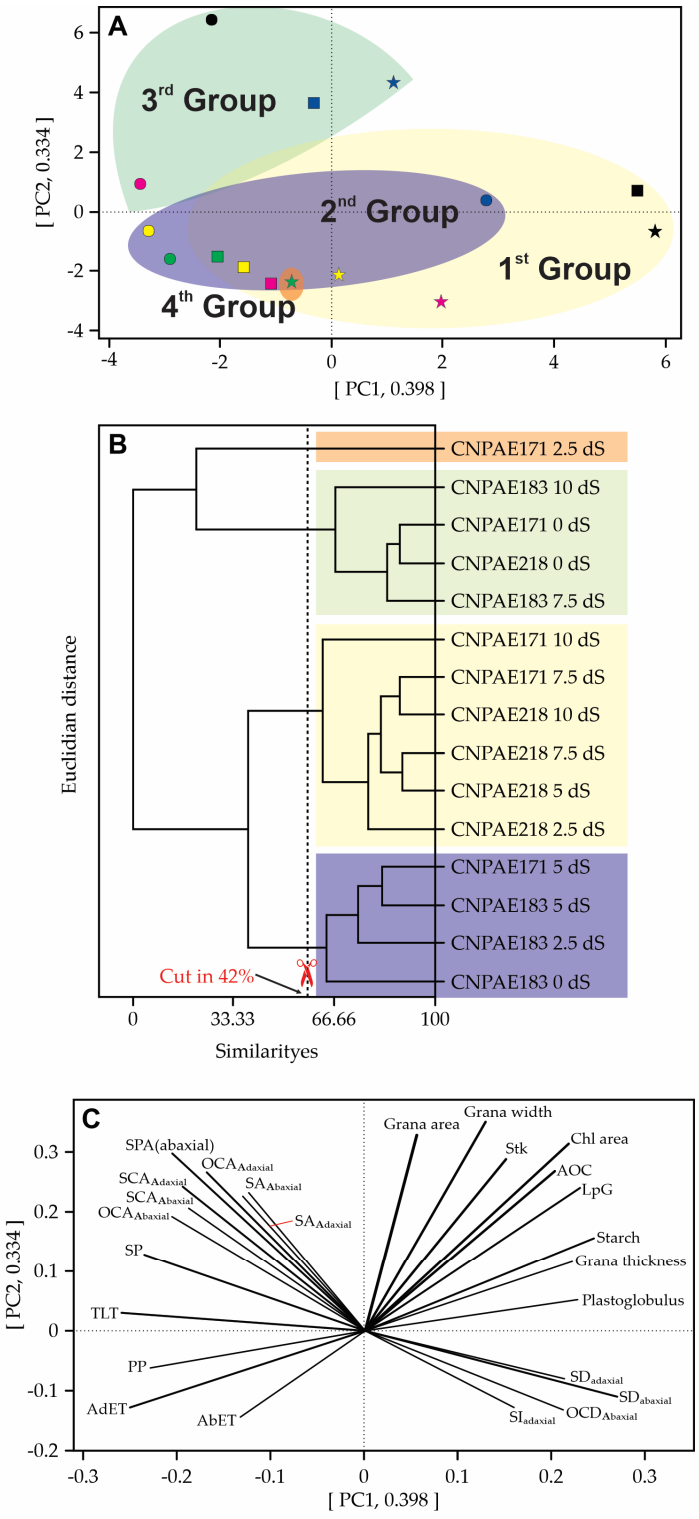

Figure 15. Multivariate analysis to assess all anatomical and ultrastructural characteristics of *Jatropha curcas* genotypes. In (**A**), all treatments are displayed in PC1 and PC2 to sh a cluster formation. In **B**, a dendrogram based on similarities between genotypes and salt treatments is shown. In (**C**), the spatial distribution of all analyzed features displays the strength of each anatomical and ultrastructural characteristic: AbET, Abaxial epidermis thickness; AdET, Adaxial epidermis thickness; Chl area, Chloroplast area; AOC, Area occupied by chloroplast; LpG, Lamellae per Grana; OCA, Ordinary cell area; OCD, Ordinary cell density; PP, palisade parenchyma; SA, stomatal area; SCA, Stomatal complex area; SD, stomatal density; SI, Stomatic index; SP, spongy parenchyma; SPA, stomatal pore area; Stk, Grana stacking; TLT, total leaf area.

 doi:10.20944/preprints202307.0048.v1

It is well established that abiotic stresses, in this case, salt stress, can cause significant changes in the leaf structure [33,34]. However, it is not well-established how salt stress acts on the leaf mesophyll, even though some authors argue that salinity causes changes in tissue thickness [4]. Different authors describe that plants of *J. curcas* under salt stress presenting a thickening of the mesophyll, sometimes more pronounced [2], sometimes less pronounced [4]. The present data agree with previous data in reporting that salt stress increases the total leaf thickness [2,4,19-23], however, in contrast to our results [35-38], other authors report that salt stress does not have any influence on leaf thickness [39]. In this point of view Taratima, *et al*. [35] and Taratima, *et al.* [40] describe that anatomical adaptations also occur under salinity stress, *e.g.* an increase in the cuticle, epidermis, and leaf thickness occurs to prevent water loss. The reduction of leaf area in salt-stressed *J. curcas* plants was previously reported [2,7,41], and this reduction leads to an increase in leaf thickness as a result of tissue condensation – more sclerophyllous leaves. In accordance with Terletskaya and Kurmanbayeva [21] the leaf thickness could be explained by an increase in cuticle thickness. Our findings, in part, disagree with those presented by Silva-Santos, *et al*. [2]. The difference between our results and Silva-Santos, *et al*. [2] results are in salt exposure. While the studies described by Silva-Santos, *et al*. [2] were evaluated after 50 hours of salt stress, this study subjects the salt exposure *J. curcas* plants for either 1 or 2 years with a basal salinity. Among the changes that can occur in plants under salt stress, the thickness of spongy parenchyma increased in plants under salt stress, but this increase was not the same for other tissues, and as a result, did not cause a significant effect of saline stress on leaf thickness [39]. Regardless of this, an increase in palisade tissue thickness is related to an increase in the number of chloroplasts as well as a decrease in the thickness of spongy tissue, which facilitates CO_2 reaching chloroplasts in the palisade parenchyma. These anatomical alterations could be an adaptation strategy to facilitate the photosynthesis process under saline stress conditions [19,22]. However, in this study, we described a positive correlation (r = 0.311) between palisade and spongy parenchyma, a negative correlation (r = -0.176) between palisade parenchyma and chloroplast area and, a non-significant correlation between palisade thickness and cell area occupied by chloroplasts (Supplementary data file).

Several plant species accumulate calcium oxalate crystals in specialized crystal idioblast cells. Labelling and genetic evidence suggest that the oxalate is derived from ascorbate [42,43]. The occurrence of calcium oxalate (CaOx) crystals is formed from endogenous oxalic acid and calcium from the environment [4]. The functions of CaOx crystals, including Ca ion regulation, mechanical support, protection against grazing and chewing insects, and metal detoxification, depending upon the amount of the crystals, morphology, and distribution within the tissues [44]. The true function of calcium crystals in stressed plants is not well documented; however, Grigore and Toma [45] describe that calcium also plays an important role in maintaining the integrity of plant cell membranes. Hunsche, *et al.* [46] describe that calcium oxalate crystals can build up a reservoir to ensure calcium supply for metabolic processes when its absorption and translocation are hindered due to environmental stresses such as salinity. Regarding this, calcium oxalate crystals form a physiological barrier to free diffusion of potentially toxic ions prevalent in a saline environment. In the present study, we verified a greater distribution of idioblast-calcium-oxalate-type crystals in 2-year-old *J. curcas* plants in comparison to their 1-year-old counterparts. On the other hand, it is quite evident that there is a reduction of idioblasts with the increase of saline concentration, as previously described for *J. curcas* [2,4] and *Grewia tenax* [46].

Plants are remarkable organisms that have evolved various strategies to cope with challenges such as seasonal drought. One crucial adaptation involves changes in hydraulic conductance (*K*p), which refers to the movement of water through the plant's vascular system [47,48]. When faced with limited water availability, plants adjust their *K*p to maintain a favourable water balance [47,49-52]. By regulating the flow of water, plants can allocate it efficiently, ensuring that essential processes like photosynthesis and nutrient uptake are sustained even in dry conditions. These adjustments in *K*p allow plants to optimize their water use, enabling them to survive and thrive in environments prone to seasonal drought. Hydraulic studies on *J. curcas* are still very scarce [12,53]. In our study, *K*p shows a pattern more or less constant, without a defined pattern, but with a tendency to decrease. Similar

 doi:10.20944/preprints202307.0048.v1

results were described in *Hordeum vulgare* [26]. Several studies have demonstrated a relationship between the water potential that induces stomatal closure and that which triggers cavitation of the stem xylem [52]. Even though *K*p did not show a very clear trend, its positive relationship with the stomatal pore area on the adaxial surface of the epidermis is visible (r = 0.339; Supplementary data file), but this is not the case with the stomata on the abaxial surface (p = 0.481). This relationship becomes clearer with a positive correlation between the potential conductivity of vessels and the stomatal area in the adaxial surface of the epidermis. Thus, the greater the vapour pressure deficit (VPD), the smaller the stomatal opening, the lower the potential conductivity, and the lower the pressure under the conductive vasculature for embolism [54]. However, the opposite premise is true; the smaller VPD with greater stomatal opening, the greater the *K*p and the greater the need to replace the water in the conducting vessels that must reduce their osmotic potential to be able to capture water. A decrease in *K*p reduces the risk of xylem embolism [55,56]. In accordance with Santana *et al*. [57] a decrease of 56% to 87% in whole-plant hydraulic conductivity, as well as a 38% decrease in total biomass, resulted in significantly low biomass water use efficiency in water deficit conditions as compared to irrigated plants [57]. Moreover, significant decreases of 57% to 65% in stem *K*p were demonstrated in water deficit plants of *J. curcas*, which were completely recovered after six days of rehydration [12]. The authors also reported no changes in *K*p in two of the ten genotypes evaluated, despite the decreases in stomatal conductance and transpiration rate, demonstrating a highly positive characteristic of water use efficiency under drought. Therefore, it is possible to suggest that some genetic materials may have the ability to recover and/or maintain *K*p by a mechanism that is still unknown. For example, in our study, the *K*p shows a positive correlation with salt exposure (time in years; r = 0.564) but does not show a positive correlation with salt stress. With these data, we can infer that *J. curcas*, as a species with a moderate tolerance to salinity, presents a plasticity that allows it to live in saline environments, since the plant established itself there and acclimatized over time, similar to previous observations for some *Cyprus* sp. [52], *Pinus ponderosa* [58], and *Eucalyptus camaldulensis* [59]. A trade-off with 'stress time' for hydraulic conductivity was previously reported in some *Cyprus* species, where, in the 1st year, any significant effect of the moderate drought treatment on hydraulic conductivity was demonstrated, instead, there are significant effects in 2nd year of study [52]. The same results were shown in *Pinus sylvestris* and *Quercus pubescens* [54]. The positive correlation between *K*p and lumen vessel area (r = 0.460) and the vessel element density (r = 0.640) allow us to infer that the pressure on the xylem permits an adaptation of the vessel elements. In accordance with Atabayeva, *et al*. [26], under salt stress, a decrease in cell size, changes in the number of stomata, and reduction in the thickness of the epidermis of leaves of the apical meristem, cortex and central cylinder diameter were shown [26]. A decrease in vascular bundle vessels as consequence to water stress is commonly associated with a lowered water potential. Also, NaCl causes an inhibition of the growth of the vascular system in a similar manner that occurs due to the water stress [26,60]. *In totum*, we speculate that with more and smaller calibre vessel elements available, the plants must control *K*p in a certain way to avoid embolism, even if this was not directly measured. A positive correlation between the *K*p *x* lumen vessel area was previously reported for *Cyprus* sp. [52], *Quercus pubes*, *Pinus sylvestris* [54], *Spergularia marina* [23], and others [60-62]. It is noteworthy that the largest vessels (*J. curcas*) are the most efficient, but they are also the most vulnerable to cavitation; so, the reduction in the lumen vessel area is a very important strategy to withstand and escape salt stress. Other key factors also contribute to the increase and decrease of resistances for the xylem, and consequently to variations in hydraulic conductance, such as the feature of secondary wall thickening, perforation plates, vessel dimensions and density [53,63]. Xu, Zhang and Li [53] analyzed the relationships between a vessel's anatomical traits and water transport inside of the xylem of *J. curcas*. They showed that, despite the xylem vessel providing a low resistance path for water transport, changes in the vessel inner diameter significantly affected the total resistance. Neves, *et al.* [64] observed that water deficit conditions affected stem and leaf xylem characteristics, such as decreases in the length and width of vessel elements and an increased frequency and density of these cells. Melo, *et al*. [4] describes the lower vessel area in salt-stressed *J. curcas* plants. Likewise Oliveira *et al*. [12] showed changes in density and the number of vessels in the stem xylem of water deficit plants of *J. curcas*,

 doi:10.20944/preprints202307.0048.v1

which directly impacted water transport. These authors also managed to demonstrate that a 34% increase in the density of vessels in a drought-tolerant genotype was associated with an increased *K*p under water deficit. Thus, *J. curcas* can be described as following a drought avoidance strategy with a conservative root system. The xylem of absorbent roots in plants under drought conditions contains only a small quantity of narrow vessels, which explains the low root *K*p [65,66]. Notwithstanding, the maximum *K*p and maximum photosynthetic rate are both closely related to the leaf vein density [28]. In general, leaf transpiration is directly related to the stomatal density and stomatal size [28,67]. Similarly, in *Toona ciliata*, the number of fine veins and stomatal density are both regulated by leaf expansion so that leaf *K*p and photosynthetic rates promoted by stomatal conductance remain proportional [68].

Stomata, the crucial structure in the plant epidermis, plays a pivotal role in regulating essential physiological processes. These stomatal pore helps to maintain an optimal balance between water loss and CO_2 uptake, particularly when faced with challenging environmental conditions. By controlling the size of their stomatal apertures, plants can modulate the rate of transpiration, thus conserving water during periods of drought or salt stress [1,2]. In this study, we characterized the leaf epidermis, both on the adaxial and abaxial surfaces. Lower stomata size and consequently, a higher density (r = -0.704), were described in this study as well as described in other studies, for *J curcas* [1,2,27], *Eucalyptus globulus* [69], *Gossypium hirsutum* [28], and other species [23,70]. Lesser stomata size and higher density were recorded as significant anatomical adaptation characteristics under drought and salinity stress to reduce transpiration [71]. Lei *et. al*. [28] described that water stress alters the stomatal density in abaxial surfaces but not in an adaxial surfaces. Our findings disagree with these authors because the stomatal density of the most stressed plants (10 dS m^{-1}) was increased both on the adaxial and abaxial surfaces, even though the abaxial epidermis is rich in reflector trichomes (Figure 10 F,G). It is important to highlight that the increase in SD was only registered in the CNPAE218 and CNPAE171 genotypes while in CNPAE183 there was a decrease (Figures 6A,B and 7A,B), as previously described for an experiment prior to this one carried out by this team [1]. However, the stomatal pore area was reduced with an increase in both of salt concentration and exposure time, the last only affecting the abaxial surface. This finding is corroborated with Hsie, *et al*. [27] and Silva-Santos, *et al.* [2] for *J. curcas* and Lei *et. al*. [28] for *Gossypium hirsutum*. Also, Lei *et. al*. [28] describe that vein density was positively and significantly correlated with stomata density on both the adaxial and abaxial surfaces. This last data disagrees with our data, which described that salt-stressed *J. curcas* plants significantly decrease the ratio of stomatal density to vein density (Supplementary data file). This may demonstrate that the xylem conduction system was not able to keep the stomata open in more severe treatments, unlike the data presented by Lei *et. al*. [28]. It should be noted that in this work, the saline stress was uninterrupted for 2 years, while in cotton [28], the plants were exposed to a water deficit for only 12 days. Noteworthy, previous researchers proposed that small stomata can rapidly respond to changes in the external environment [27,28,67,72,73].

As previously described, grana stacking is the best indicator of chloroplast integrity. We believe that in non-stressed cells, with a good source-to-sink relationship, photosynthates are produced and exported to the cytosol, where they are converted to other sugars and transported via the phloem [74]. However, phloem loading essentially depends on (i) an osmotic potential differential within the phloem vessels; (ii) utilization of photosynthate by sink organs, and (iii) a favourable transpiration current for xylem ascension which should provide water to promote the osmotic potential differences between source-to-sink [88]. The source-to-sink relationship is crucial to the phloem loaded to transport the trioses phosphate into the phloem [75,76]. Thus, the sink strength of a particular organ determines its force to mobilize photoassimilates from the source [76]. It is influenced by various factors, including the sink size or capacity of the tissue or organ to import and store further compounds from the source(s). Additionally, the sink activity, measured by the respiration rate, plays a significant role in the overall dynamics of the source-to-sink relationship. Apart from this, the management of the plant canopy also increases assimilate balance and improves the source-to-sink growth [75]. To have a difference in osmotic potential to load phloem there must be an osmotic

Preprints (www.preprints.org) | NOT PEER-REVIEWED | Posted: 4 July 2023 doi:10.20944/preprints202307.0048.v1

differential between mesophyll cells and xylem cells. For example, there was no significant correlation between $SD_{adaxial}$ to *K*p. Another observation shows that the $SD_{abaxial}$ has a smooth negative correlation with *K*p (r = -0,179) resulting in a weaker force to xylem load with water. A significant correlation exists between *K*p and the stomatal pore area of the abaxial stomata. This reflects the basic principle of photosynthesis, opening stomata to capture CO_2 for photosynthesis and losing water to the atmosphere or controlling stomatal opening for less severe times, even if this reduces net photosynthesis. [77,78]. With a lower xylem ascension, lower metabolic rates under salt stress [1] and lower sink strength, also caused by lower osmotic potential, there will be lower phloem loading. Thus, in the first moments after the onset of salt stress or in the first hours of the day, the photosynthetic rate can remain reasonable, even under salt stress and, if there are no conditions for the translocation of photoassimilates, they remain in the chloroplast and are used for the primary starch synthesis. As previously demonstrated, larger starch granules promote the destruction of thylakoid lamellae and then a secondary reduction in the photosynthetic rate [79]. Furthermore, favourable conditions must be present for phloem loading, which appear to be regulated by genes of the type CsSTS (*Cucumis sativus* stachyose synthase) [80], StSUT2 (*Spondias tuberosa* sucrose transporter 2) [81], and SWEET4 superfamily of genes [82]. However, when the metabolism is reduced, the expression of genes involved in phloem loading may also be compromised, and as a consequence, more starch granules are formed into the chloroplast [83-85].

4. Materials and Methods

4.1. Plant material and environmental conditions

Jatropha curcas, a globally cultivated plant, has gained recognition for its ability to thrive with a meager amount of water [86-90]. This remarkable attribute not only provides drought tolerance but also its impressive salt tolerance [10,91-94]. *J. curcas* can tolerate high salinity levels in the soil, making it suitable for cultivation in coastal areas and regions with saline water sources [95-97]. Additionally, this plant exhibits rapid growth, enabling it to establish itself quickly in a variety of environments. Its adaptation to harsh agroclimatic conditions further enhances its desirability as a cultivated crop. *J. curcas* is highly valued by farmers and researchers, as it offers a sustainable solution for areas facing water scarcity and challenging climatic conditions, contributing to agricultural resilience and productivity [95].

In this study, the experiments were conducted as described in detail in Pompelli, *et al.*, [1]. The global radiation intercepted by the plants varied widely during the experiment (Supplementary Figure S1), reaching 19,443 MJ m^{-2} in January 2017. However, when we consider the higher radiation intercepted by the plants in each evaluation, March 03, 2018, stands out with a higher radiation intercepted by plants (Supplementary Figure S1).

The genotype chosen was the same as presented in Pompelli *et al.* [1] and Souza, *et al.* [98], with CNPAE183, considered tolerant to salinity, and CNPAE218, considered sensitive, and JCAL171 with an intermediate tolerance. After seedling production without salt, the *J. curcas* plants were transplanted to the final site, namely 250-L barrels, filled with soil from the Petrolina region, as previously described [1]. After 30-days, *J. curcas* plants were considered the plant source and then irrigated with five salt concentrations in the irrigation water (0 dS m^{-1}, 2.5 dS m^{-1}, 5.0 dS m^{-1}, 7.5 dS m^{-1}, and 10.0 dS m^{-1}), and 5 replicates. The plant irrigation was performed by an automated irrigation system containing, for each saline concentration, a 500-L water tank, a peristaltic pump and a channel system that carried the water used for drip irrigation to the plants. All plants were irrigated every other day using dripper tubes with a flow of 2.5-L h^{-1}, having a nominal diameter of 13 mm, with two drippers per plant, spaced 0.15 m apart. Irrigation was performed for 2 hours per day by applying 10 liters $plant^{-1}$ day^{-1}. After that, all plants were cultivated for 12 or 24 months with sampling occurring in this period for all features described below.

It is worth noting that before the collection of leaf samples, some stages of leaf primordia (less than 2 cm in length) were marked with red tape to ensure that all leaves developed within the treatment period and that they were not already formed in the field before samples were taken.

Preprints (www.preprints.org) | NOT PEER-REVIEWED | Posted: 4 July 2023 doi:10.20944/preprints202307.0048.v1

4.2. Optical anatomy

Leaf fragments 5 cm^2 of the 3rd attached fully expanded leaf from the apex were sampled in 12- and 24-month stressed plants. In each plant, two leaf fragments were collected, promptly immersed in $FAA_{50\%}$ for 48 h and then stored in 70% (v/v) ethanol until analysis. Leaf samples were dehydrated in an ethylic series and embedded in plastic resin (Historesin-Leica Microsystems Nussloch, Heidelberg, Germany, part number 7592). Following this, all samples were processed as described in detail in Mendes, *et al*. [99] according to the scheme presented in Supplementary Figure S3. For each sample, 100 images were captured by a digital camera (Mikrosysteme Vertrieb GmbH, model ICC50 HD; Wetzlar, Germany) and interfaced with a computer. To estimate the potential hydraulic conductivity (*Kp*), the principles of the Hagen-Poiseuille equation were done using equation 1.

$$K_p = \left(\frac{\pi p_w}{128\eta}\right) x\ VD\ x\ D_h^4 \qquad Eq.1$$

where *Kp* is the potential specific stem conductivity, η is the viscosity of water at 20ºC (1.002 x 10^{-3} Pa), ρ_w is the density of water at 20ºC (998.2 kg m^{-3}), VD is the vessel density and D_h is the hydraulically weighted vessel diameter (in m). Since vessels are not exactly circular, the diameter of each vessel was calculated as the mean of the minimum and maximum diameters. The average D_h was calculated as well as Sterck *et al*. [54]. As recommended by Scholz *et al*. [60] we measured at least 50 vessels per photomicrograph, resulting in 250 vessels (5 repetitions) per treatment.

4.3. Scanning electron microscopy

Leaf fragments ~0.5 cm^2 of the 3rd attached fully expanded leaf from the apex were sampled in 12- and 24-month stressed plants and immediately fixed in a Karnovsky solution [100], prepared in 0.1 M cacodylate buffer (sodium cacodylate trihydrate, Sigma Aldrich, St. Louis, USA, part number C4945), pH 7.4 and 2.5% glutaraldehyde (Sigma Aldrich, part number G5882) for 60 h at 4ºC. All preparation steps were done as described in detail in Pompelli *et al*. [1] with modifications proposed by Pompelli *et al*. [101]. For each sample, 50 images were captured by x-ray (EDS) IXRF-Iridium Ultra Version 1.3, Model 550i. For the stomatal area, stomatal pore area, stomatal complex area, ordinary cell area and its ratios the methodology was schematized in Supplementary Figure S4. To this analysis, a minimum sampling size (n) was calculated to determine how many cells must be measured. This is calculated by using the formula below to find the number of cells to be measured within the total number of cells available. In this case, we used the tolerable error rate of 15% as recommended by Lin and Huang [102]

$$n_{sample} = \frac{ECN * \left(\frac{100}{e}\right)^2}{ECN * \left(\frac{100}{e}\right)^2 + ECN + \left(\frac{100}{e}\right)^2} \qquad Eq.2$$

where: ECN. Epidermal cells number; e. tolerable error rate

4.4. Transmission electron microscopy

Leaf segments of approximately 0.5 mm in length were taken from the middle section of the 3rd attached fully expanded leaf from the apex and were sampled for the 12- and 24-month stressed plants and immediately fixed in Karnovsky solution [100], prepared with 2% glutaraldehyde in 0.1 M sodium cacodylate buffer pH 7.4 [100]. Then, all leaf fragments were processed as described in detail in Mendes *et. al*. [99]. For each sample 25 ultra-thin cuts (5 μm^2) from at least 5 replicates were obtained with a transmission electron microscope, 50 kV, with a coupled digital camera (EM 109, Carl Zeiss Microscopy Ltd., Jena, Germany).

4.5. Experimental Design and Statistical Analysis

The experiments were conducted in a completely randomized design composed of 3 *J. curcas* genotypes (CNPAE183, CNPAE218, and CNPAE171), 5 electric conductivities in the irrigation water (0 dS m^{-1}, 2.5 dS m^{-1}, 5.0 dS m^{-1}, 7.5 dS m^{-1}, and 10.0 dS m^{-1}) and one and two years old *J. curcas* stressed plants. All data were processed by Two way ANOVA, in SigmaPlot for Windows v. 14.0 (Systat

Software, Inc., San Jose, CA, USA). The principal component analysis was estimated after a multivariate analysis for all analyzed features in Minitab 18.1 (Minitab, Inc., Chicago, IL, USA). Heat maps were used to compare the mean of each treatment, using the control (0 dS m^{-1}) as a reference. After log_2 transformation, the false colour method was used, including a colour scale. The heat maps were constructed using Microsoft® Office 360 (Microsoft Corporation, Redmond, WA, USA) and Corel DRAW Graphics Suite X8 (Corel Corporation, Ottawa, ON, Canada).

5. Conclusions

Our findings suggest that *Jatropha curcas* plants exposed to salt stress exhibit increased mesophyll thickness, characterized by more compact cells in the spongy parenchyma and occasionally a bistratified adaxial epidermis surface. The abaxial epidermis surface contains a higher stomata density and ordinary cell density, often accompanied by reflective trichomes. The rise in stomatal density appears to be regulated by a reduction in leaf area and is positively correlated with the potential conductivity of vessels. This potential conductivity serves as a driving force for water movement from leaves to roots and soil. The decrease in leaf area in salt-stressed *J. curcas* plants leads to both lower and higher stomatal density on the surfaces of both epidermises. This variation in stomatal density is likely a response to salt stress. Notably, our main findings suggest that potential conductivity may be associated with certain chloroplast characteristics, including variations in chloroplast density. Salt stress promotes a decrease or increase in chloroplast density as the plant tries to sustain photosynthesis and ATP production under stressful conditions. However, further studies are necessary to provide additional evidence for this hypothesis.

Supplementary Materials: The following supporting information can be downloaded at: www.mdpi.com/xxx/s1, Supplementary Figures S1–S4.

Author Contributions: Conceptualization, M.F.P.; J.D.P.; W.L.A.; methodology, M.F.P.; J.D.P.; software, M.F.P.; validation, M.F.P.; J.D.P.; W.L.A.; formal analysis, M.F.P.; J.D.P.; investigation, M.F.P.; J.D.P.; W.L.A. writing—original draft preparation, M.F.P.; J.D.P.; J.D.J.N.; A.J.O.; L.A.R.P.; Y.Y.P.R.; writing—review and editing, M.F.P.; W.L.A.; supervision, J.D.J.N.;A.J.O.; L.A.R.P.; W.L.A.; project administration, M.F.P.; funding acquisition, M.F.P.; W.L.A. All authors have read and agreed to the published version of the manuscript.

Funding: This research was funded by National Council for Scientific and Technological Development (CNPq-Brazil, Grant 404357/2013-0). We thank the scholarships granted by CNPq-Brazil (Grants 163524/2017-3 to MFP). Research fellowship granted by CNPq-Brazil to WLA is also gratefully acknowledged.

Acknowledgments: The authors thanks to Embrapa Agroenergia (Brasília, DF, Brazil) for donating the *J. curcas* seeds and Embrapa Semiárido, Petrolina, PE, Brazil for providing all infrastructure for the assembly of this study. In addition, the authors extend special thanks to Nucleus of Microscopy and Microanalyses, at the Universidade Federal de Viçosa for technical assistance.

Conflicts of Interest: The authors declare no conflict of interest.

References

1. Pompelli, M.F.; Ferreira, P.P.B.; Chaves, A.R.M.; Figueiredo, R.C.Q.Q.; Martins, A.O.; Jarma-Orozco, A.; Batista-Silva, W.; Endres, L.; Araújo, W.L. Physiological, metabolic, and stomatal adjustments in response to salt stress in *Jatropha curcas*. *Plant Physiol Bioch* **2021**, *168*, 116-127, doi:10.1016/j.plaphy.2021.09.039.
2. Silva-Santos, L.; Corte-Real, N.; Dias-Pereira, J.; Figueiredo, R.C.B.Q.; Endres, L.; Pompelli, M.F. Salinity shock in *Jatropha curcas* leaves is more pronounced during recovery than during stress time. *Braz J Develop* **2019**, *5*, 11359-11369, doi:10.34117/bjdv5n8-033.
3. Acosta-Motos, J.R.; Ortuño, M.F.; Bernal-Vicente, A.; Diaz-Vivancos, P.; Sanchez-Blanco, M.J.; Hernandez, J.A. Plant responses to salt stress: adaptive mechanisms. *Agronomy* **2017**, *7*, 18, doi:10.3390/agronomy7010018.
4. Melo, G.M.; da Cunha, P.C.; Pereira, J.A.F.; Willadino, L.; Ulisses, C. Anatomical changes in the leaves and roots of *Jatropha curcas* L. cultivated under saline stress. *Rev Ciência Agr* **2011**, *42*, 670-674, doi:10.1590/S1806-66902011000300013.
5. Ashraf, M.; Harris, P. Photosynthesis under stressful environments: an overview. *Photosynthetica* **2013**, *51*, 163-190, doi:10.1007/s11099-013-0021-6.

6. Arcoverde, G.B.; Rodrigues, B.M.; Pompelli, M.F.; Santos, M.G. Water relations and some aspects of leaf metabolism of *Jatropha curcas* young plants under two water deficit levels and recovery. *Braz J Plant Physiol* **2011**, *23*, 123-130.
7. Corte-Real, N.; Miranda, P.V.V.C.; Endres, L.; Souza, E.R.; Pompelli, M.F. Tolerance to salinity in *Jatropha curcas* are genotype-dependent. *Braz J Develop* **2019**, *5*, 22169-22199, doi:10.34117/bjdv5n10-347.
8. Gomes, M.F.C.; Binneck, E.; Ferreira-Neto, J.R.C.; Luz, G.A.; Benko-Iseppon, A.M.; Pompelli, M.F.E., L.; Kido, É.A. Transcriptome analysis uncovers the *Jatropha curcas* L. transportome after NaCl (150 mM) exposure. *Physiol Plant* **2021**, *in press*.
9. Pompelli, M.F.; Jarma-Orozco, A.; Rodrígues-Páez, L.A. Salinity in *Jatropha curcas*: a review of physiological, biochemical, and molecular factors involved. *Agriculture* **2022**, *12*, 594, doi:10.3390/agriculture12050594.
10. Bezerra-Neto, E.; Coelho, J.B.M.; Jarma-Orozco, A.; Rodríguez-Páez, L.A.; Pompelli, M.F. Modulation of photosynthesis under salinity and the role of mineral nutrients in *Jatropha curcas* L. *J Agron Crop Sci* **2021**, *208*, 314-334, doi:10.1111/jac.12583.
11. Melcher, P.J.; Holbrook, N.M.; Burns, M.J.; Zwieniecki, M.A.; Cobb, A.R.; Brodribb, T.J.; Sack, L. Measurements of stem xylem hydraulic conductivity in the laboratory and field. *Methods Ecol Evol* **2012**, *3*, 685-694, doi:10.1111/j.2041-210X.2012.00204.x.
12. Oliveira, P.S.; Pereira, L.S.; Silva, D.C.; Souza Júnior, J.O.; Laviola, B.G.; Gomes, F.P. Hydraulic conductivity in stem of young plants of *Jatropha curcas* L. cultivated under irrigated or water deficit conditions. *Ind Crop Prod* **2018**, *116*, 15-23, doi:10.1016/j.indcrop.2017.12.066.
13. Fernández-Marín, B.; Gulías, J.; Figueroa, C.M.; Iñiguez, C.; Clemente-Moreno, M.J.; Nunes-Nesi, A.; Fernie, A.R.; Cavieres, L.A., .; Bravo, L.A.; García-Plazaola, J.I.; et al. How do vascular plants perform photosynthesis in extremeenvironments? An integrative ecophysiological andbiochemical story. *Plant J* **2020**, *101*, 979-1000, doi:10.1111/tpj.14694.
14. Gauhl, E.; Björkman, O. Simultaneous measurements on the effect of oxygen concentration on water vapor and carbon dioxide exchange in leaves. *Planta* **1969**, *88*, 187-191, doi:10.1007/BF01391125.
15. Lin, J.; Li, J.P.; Yuan, F.; Yang, Z.; Wang, B.S.; Chen, M. Transcriptome profiling of genes involved in photosynthesis in *Elaeagnus angustifolia* L. under salt stress. *Photosynthetica* **2018**, *56*, 998-1009, doi:10.1007/s11099-018-0824-6.
16. Sivakumar, P.; Sharmila, P.; Pardha-Saradhi, P. Proline alleviates salt-stress-induced enhancement in Ribulose-1,5-bisphosphate oxygenase activity. *Biochem Biophys Res Commun* **2000**, *279*, 512-515, doi:10.1006/bbrc.2000.4005.
17. Choudhury, F.K.; Rivero, R.M.; Blumwald, E.; Mittler, R. Reactive oxygen species, abiotic stress and stress combination. *Plant J* **2016**, *90*, 856-867, doi:10.1111/tpj.13299.
18. Muchate, M.S.; Nikalje, G.C.; Rajurkar, N.S.; Suprasanna, P.; Nikam, T.D. Plant salt stress: adaptive responses, tolerance mechanism and bioengineering for salt tolerance. *Bot Rev* **2016**, *82*, 371-406, doi:10.1007/s12229-016-9173-y.
19. El-Banna, M.F.; Abdelaal, K.A.A. Response of strawberry plants grown in the hydroponic system to pretreatment with H_2O_2 before exposure to salinity stress. *J Plant Production, Mansoura Univ* **2018**, *9*, 989-1001.
20. Bongi, G.; Loreto, F. Gas-exchange properties of saltstressed olive (*Olea europea* L.) leaves. *Plant Physiol* **1989**, *90*, 1408-1416, doi:10.1104/pp.90.4.1408.
21. Terletskaya, N.; Kurmanbayeva, M. Change in leaf anatomical parameters of seedlings of different wheat species under conditions of drought and salt stress. *Pak J Bot* **2017**, *49*, 857-865.
22. Toscano, S.; Ferrante, A.; Tribulato, A.; Romano, D. Leaf physiological and anatomical responses of *Lantana* and *Ligustrum* species under different water availability. *Plant Physiol Bioch* **2018**, *127*, 380-392, doi:10.1016/j.plaphy.2018.04.008.
23. Akcin, T.A.; Akcin, A.; Yalcin, E. Anatomical adaptations to salinity in *Spergularia marina* (Caryophyllaceae) from Turkey. *Proc Nat Acad Sci, India Sect B Biol Sci* **2014**, *85*, 625-634, doi:10.1007/s40011-014-0386-8.
24. Trebst, A.; Tsujimoto, H.; Arnon, D. Separation of light and dark phases in the photosynthesis of isolated chloroplasts. *Nature* **1958**, *182*, 351-355, doi:10.1038/182351a0.
25. Buchanan, B.B.; Wolosiuk, R.A. Photosynthesis: the carbon reactions. In *Plant Physiology, 5th edition*, Taiz, L., Zeiger, E., Eds.; Sinauer Associates, Inc.: Sunderland, USA, 2010; pp. 199-242.

26. Atabayeva, S.; Nurmahanova, A.; Minocha, S.; Ahmetova, A.; Kenzhebayeva, S.; Aidosova, S.; Nurzhanova, A.; Zhardamalieva, A.; Asrandina, S.; Alybayeva, R.; et al. The effect of salinity on growth and anatomical attributes of barley seedling (*Hordeum vulgare* L.). *Afr J Biotechnol* **2013**, *12*, 2366-2377, doi:10.5897/AJB2013.12161.
27. Hsie, B.S.; Mendes, K.R.; Antunes, W.C.; Endres, L.; Campos, M.L.O.; Souza, F.C.; Santos, N.D.; Singh, B.; Arruda, E.C.P.; Pompelli, M.F. *Jatropha curcas* L. (Euphorbiaceae) modulates stomatal traits in response to leaf-to-air vapor pressure deficit. *Biomass Bioenerg* **2015**, *81*, 273-281, doi:10.1016/j.biombioe.2015.07.014.
28. Lei, Z.Y.; Han, J.M.; Yi, X.P.; Zhang, W.F.; Zhang, Y.L. Coordinated variation between veins and stomata in cotton and its relationship with water-use efficiency under drought stress. *Photosynthetica* **2018**, *56*, 1326-1335, doi:10.1007/s11099-018-0847-z.
29. Leigh, A.; Sevanto, S.; Close, J.D.; Nicotra, A.B. The influence of leaf size and shape on leaf thermal dynamics: does theory hold up under natural conditions? *Plant Cell Environ* **2016**, *40*, 237-248.
30. Pompelli, M.F.; Mendes, K.R.; Ramos, M.V.; Santos, J.N.B.; Youssef, D.T.A.; Pereira, J.D.; Endres, L.; Jarma-Orozco, A.; Solano-Gomes, R.; Jarma-Arroyo, B.; et al. Mesophyll thickness and sclerophylly among *Calotropis procera* morphotypes reveal water-saved adaptation to environments. *J Arid Land* **2019**, *11*, 795-810, doi:10.1007/s40333-019-0016-7.
31. Peguero-Pina, J.J.; Sancho-Knapik, D.; Barrón, E.; Camarero, J.J.; Vilagrosa, A.; Gil-Pelegrín, E. Morphological and physiological divergences within *Quercus ilex* support the existence of different ecotypes depending on climatic dryness. *Ann Bot* **2014**, *114*, 301-313, doi:10.1093/aob/mcu108.
32. Gil-Pelegrín, E.; Saz, M.A.; Cuadrat, J.M.; Peguero-Pina, J.J.; Sancho-Knapik, D. Oaks Under Mediterranean-Type Climates: Functional Response to Summer Aridity. In *Oaks Physiological Ecology. Exploring the Functional Diversity of Genus Quercus L.*, Gil-Pelegrín, E., Peguero-Pina, J.J., Sancho-Knapik, D., Eds.; Springer: London, 2017; pp. 137-193.
33. Fahn, A. *Plant Anatomy. 2nd edition*, 2nd ed.; Butterworth Heinemann: Oxford,USA, 1990; p. 588.
34. Evert, R.F. *Esau's Plant Anatomy - meristems, cells, and tissues of tre plant body - their structures, function and development. 3rd edition*; John Wiley & Sons, Inc.: New Jersey, 2013; p. 624.
35. Taratima, W.; Samattha, C.; Maneerattanarungroj, P.; Trunjaruen, A. Physiological and anatomical response of rice (*Oryza sativa* L.) 'Hom Mali Daeng' at different salinity stress levels. *Acta Agrobot* **2023**, *76*, 764, doi:10.5586/aa.764.
36. Ola, H.; Elbar, A.; Farag, E.; Eisa, S.S.; Habib, S.A. Morpho-anatomical changes in salt stressed kallar grass (*Leptochloa fusca* L. Kunth). *J Agric Biol Sci* **2012**, *8*, 158-166.
37. Barhoumi, Z.; Djebali, W.; Chaïbi, W.; Abdelly, C.; Smaoui, A. Salt impact on photosynthesis and leaf ultrastructure of *Aeluropus littoralis*. *J Plant Res* **2007**, *120*, 529-537, doi:10.1007/s10265-007-0094-z.
38. Bastias, E.; Gonzales-Moro, M.B.; Gonzales-Murua, C. *Zea mays* L. amylacea from the Lluta Valley (Arica Chile) tolerates salinity stress when high levels of boron are available. *Plant Soil* **2005**, *267*, 73-84, doi:10.1007/s11104-005-4292-y.
39. Clemente-Moreno, M.J.; Gago, J.; Díaz-Vivancos, P.; Bernal, A.; Miedes, E.; Bresta, P.; Liakopoulos, G.; Fernie, A.R.; Hernández, J.A.; Flexas, J. The apoplastic antioxidant system and altered cell wall dynamics influence mesophyll conductance and the rate of photosynthesis. *Plant J* **2019**, *99*, 1031-1046, doi:10.1111/tpj.14437.
40. Taratima, W.; Ritmaha, T.; Jongrungklang, N.; Maneerattanarungroj, P.; Kunpratum, N. Effect of stress on the leaf anatomy of sugarcane cultivars with different drought tolerance (*Saccharum officinarum*, Poaceae). *Rev Biol Trop* **2020**, *68*, 1159-1170, doi:10.15517/rbt.v68i4.41031.
41. Cavalcante, P.G.S.; Santos, C.M.; Filho, H.C.L.W.; Avelino, J.R.L.; Endres, L. Morpho-physiological adaptation of *Jatropha curcas* L. to salinity stress. *Aust J Crop Sci* **2018**, *12*, 563-571, doi:10.21475/ajcs.18.12.04.pne835.
42. Keates, S.E.; Tarlyn, N.M.; Loewus, F.A.; Franceschi, V.R. L-Acorbic acid and L-galactose are sources for oxalic acid and calcium oxalate in *Pistia stratiotes*. *Phytochem* **2000**, *53*, 433-440, doi:10.1016/S0031-9422(99)00448-3.
43. Nakata, P.; McConn, M. Isolated *Medicago truncatula* mutants with increased calcium oxalate crystal accumulation have decreased ascorbic acid levels. *Plant Physiol Biochem* **2007**, *45*, 216-220, doi:10.1016/j.plaphy.2007.01.013.

44. Masrahi, Y.; Al-Namazi, A.; Alammari, B.; Alturki, T. Adaptations facilitate the invasion of *Cylindropuntia rosea* (DC.) Backeb. (Cactaceae) in the highlands of southwestern Saudi Arabia. *Plant Signal Behav* **2022**, *17*, 2144593, doi:10.1080/15592324.2022.2144593.
45. Grigore, M.N.; Toma, C. Ecological anatomy investigation related to some halophyte species from Moldovia. *Rom J Biol - Plant Biol* **2008**, *53*, 23-30.
46. Hunsche, M.; Bürling, K.; Saied, A.S.; Schmitz-Eiberger, M.; Sohail, M.; Gebauer, J.; Noga, G.; Buerkert, A. Effects of NaCl on surface properties, chlorophyll fluorescence and light remission, and cellular compounds of *Grewia tenax* (Forssk.) Fiori and *Tamarindus indica* L. leaves. *Plant Growth Regul* **2010**, *61*, 253-263, doi:10.1007/s10725-010-9473-x.
47. Tsuda, M.; Tyree, M.T. Plant hydraulic conductance measured by the high pressure flow meter in crop plants. *J Exp Bot* **2000**, *51*, 823-828, doi:10.1093/jexbot/51.345.823.
48. Poorter, L.; McDonald, I.; Alarcón, A.; Fichtler, E.; Licona, J.-C.; Peña-Claros, M.; Sterck, F.; Villegas, Z.; Sass-Klaassen, U. The importance of wood traits and hydraulic conductance for the performance and life history strategies of 42 rainforest tree species. *New Phytol* **2010**, *185*, 481-492, doi:10.1111/j.1469-8137.2009.03092.x.
49. Dodd, I.C. Abscisic acid and stomatal closure: a hydraulic conductance conundrum? *New Phytol* **2013**, *197*, 6-8, doi:10.1111/nph.12052.
50. Meinzer, F.; Grantz, D. Coordination of stomatal, hydraulic, and canopy boundary layer properties: Do stomata balance conductances by measuring transpiration? *Physiol Plant* **1991**, *83*, 324-329.
51. North, G.B.; Brinton, E.K.; Browne, M.G.; Gillman, M.G.; Roddy, A.B.; Kho, T.L.; Wang, E.; Fung, V.A.; Brodersen, C.R. Hydraulic conductance, resistance, and resilience: how leaves of a tropical epiphyte respond to drought. *Am J Bot* **2019**, *106*, 943-957, doi:10.1002/ajb2.1323.
52. Ladjal, M.; Huc, R.; Ducrey, M. Drought effects on hydraulic conductivity and xylem vulnerability to embolism in diverse species and provenances of Mediterranean cedars. *Tree Physiol* **2005**, *25*, 1109-1117, doi:10.1093/treephys/25.9.1109.
53. Xu, T.; Zhang, L.; Li, Z. Computational fluid dynamics model and flow resistance characteristics of *Jatropha curcas* L xylem vessel. *Sci Rep* **2020**, *10*, 14728, doi:10.1038/s41598-020-71576-9.
54. Sterck, F.J.; Zweifel, R.; Sass-Klaassen, U.; Chowdhury, Q. Persisting soil drought reduces leaf specific conductivity in Scots pine (*Pinus sylvestris*) and pubescent oak (*Quercus pubescens*). *Tree Physiol* **2008**, *28*, 529-536, doi:10.1093/treephys/28.4.529.
55. Linton, M.J.; Sperry, J.S.; D.G., W. Limits to water transport in *Juniperus osteosperma* and *Pinus edulis*: implications for drought tolerance and regulation of transpiration. *Funct Ecol* **1998**, *12*, 906-911, doi:10.1046/j.1365-2435.1998.00275.x.
56. Hacke, U.G.; Sperry, J.S.; Pittermann, J. Drought experience and cavitation resistance in six shrubs from the Great Basin, Utah. *Basic Appl Ecol* **2000**, *1*, 31-41, doi:10.1078/1439-1791-00006.
57. Santana, T.A.; Oliveira, P.S.; Silva, L.D.; Laviola, B.G.F.; de Almeida, A.-A.; Gomes, F.P. Water use efficiency and consumption in different Brazilian genotypes of *Jatropha curcas* L. subjected to soil water deficit. *Biomass Bioenerg* **2015**, *75*, 119-125, doi:10.1016/j.biombioe.2015.02.008.
58. Maherali, H.; E.H., D. Xylem conductivity and vulnerability to cavitation of ponderosa pine growing in contrasting climates. *Tree Physiol* **2000**, *20*, 859-868, doi:10.1093/treephys/20.13.859.
59. Franks, P.J.; Gibson, A.; Bachelard, E.P. Xylem permeability and embolism susceptibility in seedlings of *Eucalyptus camaldulensis* Dehnh. from two different climatic zones. *Aust J Plant Physiol* **1995**, *22*, 15-21.
60. Scholz, A.; Klepsch, M.; Karimi, Z.; Jansen, S. How to quantify conduits in wood? *Front Plant Sci* **2013**, *4*, 56, doi:10.3389/fpls.2013.00056.
61. Tyree, M. Dynamic measurements of root hydraulic conductance using a high pressure flowmeter in the laboratory and field. *J of Exp Bot* **1995**, *46*, 83-94.
62. Kozlowski, T.T. Responses of woody plants to flooding and salinity. *Tree Physiol* **1997**, *17*, 490, doi:10.1093/treephys/17.7.490.
63. Charrier, G.; Torres-Ruiz, J.M.; Badel, E.; Burlett, R.; Choat, B.; Cochard, H.; Delmas, C.E.L.; Domec, J.C.; Jansen, S.; King, A.; et al. Evidence for hydraulic vulnerability segmentation and lack of xylem refilling under tension. *Plant Physiol* **2016**, *172*, 1657-1668, doi:10.1104/pp.16.01079.
64. Neves, E.L.; Funch, L.S.; Viana, B.F. Comportamento fenológico de três espécies de Jatropha (Euphorbiaceae) da Caatinga, semi-árido do Brasil. *Rev Bras Bot* **2010**, *33*, 155-166.

65. Krishnamurthy, L.; Zaman-Allah, M.; Marimuthu, S.; Wani, S.P.; Kesava Rao, A.V.R. Root growth in Jatropha and its implications for drought adaptation. *Biomass Bioenerg* **2012**, *39*, 247-252, doi:10.1016/j.biombioe.2012.01.015.
66. Tavecchio, N.; Reinoso, H.; Ruffini Castiglione, M.; Spanò, C.; Pedranzani, H.E. Anatomical studies of two *Jatropha* species with importance for biodiesel production. *J Agric Sci* **2016**, *8*, 84-94, doi:10.5539/jas.v8n9p84.
67. Drake, P.L.; Froend, R.H.; Franks, P.J. Smaller, faster stomata: scaling of stomatal size, rate of response, and stomatal conductance. *J Exp Bot* **2013**, *64*, 495-505, doi:10.1093/jxb/ers347.
68. Carins, M.R.; Jordan, G.J.; Brodribb, T.J. Differential leaf expansion can enable hydraulic acclimation to sun and shade. *Plant Cell Environ* **2012**, *35*, 1407-1418, doi:10.1111/j.1365-3040.2012.02498.x.
69. Franks, P.J.; Drake, P.L.; Beerling, D.J. Plasticity in maximum stomatal conductance constrained by negative correlation between stomatal size and density: an analysis using *Eucalyptus globulus*. *Plant Cell Environ* **2009**, *32*, 1737-1748, doi:10.1093/jxb/ers347.
70. Rahman, A.A.N.S.; Rahman, M.; Shimanto, M.H.; Kibria, M.G.; Islam, M.A. Stomatal size and density trade-off varies with leaf phenology and species shade tolerance in a South Asian moist tropical forest. *Funct Plant Biol* **2022**, *49*, 307-318, doi:10.1071/FP21159.
71. Hameed, M.; Ashraf, M.; Naz, N.; Al-Qurainy, F. Anatomical adaptations of *Cynodon dactylon* (L.) Pers. from the salt range Pakistan to salinity stress. I. Root and stem anatomy. *Pak J Bot* **2010**, *42*, 279-289.
72. Xu, Z.; Zhou, G. Responses of leaf stomatal density to water status and its relationship with photosynthesis in a grass. *J Exp Bot* **2008**, *59*, 3317-3325, doi:10.1093/jxb/ern185.
73. Zhang, S.B.; Guan, Z.J.; Sun, M.; Zhang, J.-J.; Cao, K.-F.; Hu, H. Evolutionary association of stomatal traits with leaf vein density in Paphiopedilum, Orchidaceae. *PLoS ONE* **2012**, *7*, e40080, doi:10.1371/journal.pone.0040080.
74. Dunford, S. Translocation in the Phloem. In *Plant Physiology 5th edition*, Taiz, L., Zeiger, E., Eds.; Sinauer Associates Inc.: Sunderland, MA, USA, 2010; pp. 271-303.
75. DaMatta, F.M.; Cunha, R.L.; Antunes, W.C.; Martins, S.C.V.; Araujo, W.L.; Fernie, A.R.; Moraes, G.A.B.K. In field-grown coffee trees source-sink manipulation alters photosynthetic rates, independently of carbon metabolism, via alterations in stomatal function. *New Phytol* **2008**, *178*, 348-357, doi:10.1111/j.1469-8137.2008.02367.x.
76. Smith, M.R.; Rao, I.M.; Merchant, A. Source-sink relationships in crop plants and their influence on yield development and nutritional quality. *Front Plant Sci* **2018**, *9*, 1889, doi:10.3389/fpls.2018.01889.
77. Hovenden, M.J.; Shimanski, L.J. Genotypic differences in growth and stomatal morphology of Southern Beech, *Nothofagus cunninghamii*, exposed to depleted CO_2 concentration. *Aust J Plant Physiol* **2000**, *27*, 281-287.
78. Pandey, R.; Chacko, P.M.; Choudhary, M.L.; Prasad, K.V.; Pal, M. Higher than optimum temperature under CO_2 enrichment influences stomata anatomical characters in rose (*Rosa hybrida*). *Sci Hortic-Amsterdam* **2007**, *113*, 74-81.
79. Zhai, L.; Yan, A.; Shao, K.; Wang, S.; Wang, Y.; Chen, Z.-H.; Xu, J. Large vascular bundle phloem area 4 enhances grain yield and quality in rice via source–sink–flow. *Plant Physiol* **2023**, *191*, 317-334, doi:10.1093/plphys/kiac461.
80. Haibo, D.; Zhang, W.; Hua, B.; Zhu, Z.; Zhang, J.; Zhang, Z. Cucumber STACHYOSE SYNTHASE is regulated by its cis-antisense RNA asCsSTS to balance source–sink carbon partitioning. *Plant Cell* **2023**, *35*, 435-452, doi:10.1093/plcell/koac317.
81. Miehe, W.; Czempik, L.; Klebl, F.; Lohaus, G. Sugar concentrations and expression of SUTs suggest active phloem loading in tall trees of *Fagus sylvatica* and *Quercus robur*. *Tree Physiol* **2023**, *43*, 805-816, doi:10.1093/treephys/tpac152.
82. Chen, L.; Ganguly, D.R.; Shafik, S.H.; Danila, F.; Grof, C.P.L.; Sharwood, R.E.; Furbank, R.T. The role of SWEET4 proteins in the post-phloem sugar transport pathway of *Setaria viridis* sink tissues. *J Exp Bot* **2023**, *74*, 2968-2986, doi:10.1093/jxb/erad076.
83. Taylor, A.O.; Craig, A.S. Plants under climatic stress: II. low temperature, high light effects on chloroplast ultrastructure. *Plant Physiol* **1971**, *47*, 719-725, doi:10.1104/pp.47.5.719.
84. Ackerson, R.C.; Hebert, E.R. Osmoregulation in cotton in response to water stress : I. alterations in photosynthesis, leaf conductance, translocation, and ultrastructure. *Plant Physiol* **1981**, *67*, 484-488, doi:10.1104/pp.67.3.484.

85. Capellades, M.; Lemeur, R.; Debergh, P. Effects of sucrose on starch accumulation and rate of photosynthesis in rosa cultured in vitro. *Plant Cell Tiss Organ Cult* **1991**, *25*, 21-26, doi:10.1007/BF00033908.
86. Achten, W.M.J.; Maes, W.H.; Reubens, B.; Mathijs, E.; Singh, V.P.; Verchot, L.; Muys, B. Biomass production and allocation in *Jatropha curcas* L. seedlings under different levels of drought stress. *Biomass Bioenerg* **2010**, *34*, 667-676, doi:DOI. 10.1016/j.biombioe.2010.01.010.
87. Díaz-López, L.; Gimeno, V.; Simón, I.; Martínez, V.; Rodrígues-Ortega, W.M.; García-Sánchez, F. *Jatropha curcas* seedlings show a water conservation strategy under drought conditions based on decreasing leaf growth and stomatal conductance. *Agr Water Manage* **2012**, *105*, 48-56.
88. Pompelli, M.F.; Barata-Luís, R.M.; Vitorino, H.S.; Gonçalves, E.R.; Rolim, E.V.; Santos, M.G.; Almeida-Cortez, J.S.; Endres, L. Photosynthesis, photoprotection and antioxidant activity of purging nut under drought deficit and recovery. *Biomass Bioenerg* **2010**, *34*, 1207-1215, doi:10.1016/j.biombioe.2010.03.011.
89. Silva, L.D.; Gomes, F.P.; Oliveira, P.S.; Almeida, F.R.; Pirovani, C.P.; Laviola, B.G.; Amaral, J.F.T. Plasticity of photosynthetic metabolism in Jatropha curcas genotypes under water stress. *Gen Mol Res* **2019**, *18*, 1-17, doi:10.4238/gmr18228
90. Cabrales-Rodríguez, R.; Betancur-Hurtado, C.A.; Rodríguez-Páez, L.A. *Cultivo del piñón (Jatropha curcas L.); manejo nutricional y usos en Córdoba, Colombia*; Universidad de Córdoba: Montería, Colombia, 2019; p. 88.
91. Cabral, G.A.L.; Binneck, E.; Souza, M.C.P.; Silva, M.D.; Ferreira Neto, J.R.C.; Pompelli, M.F.; Endres, L.; Kido, E.A. First expressed TFome of physic nut (*Jatropha curcas* L.) after salt stimulus. *Plant Mol Biol Rep* **2020**, *38*, 189-208, doi:10.1007/s11105-019-01187-w.
92. Campos, M.L.O.; Hsie, B.S.; Granja, J.A.A.; Correia, R.M.; Silva, S.R.S.; Almeida-Cortez, J.S.; Pompelli, M.F. Photosynthesis and antioxidant activity mechanisms in *Jatropha curcas* L. under salt stress. *Braz J Plant Physiol* **2012**, *24*, 55-67.
93. Dorta-Santos, M.A.; Barriola, I.; Wassner, D.F.; Ploschuk, E.L. Photosynthesis, fluorescence and mesophyll conductance responses to increasing salinity levels in *Jatropha curcas* at early vegetative stages. *J Agron Crop Sci* **2020**, *206*, 52-63, doi:10.1111/jac.12373.
94. Gadelha, C.G.; Miranda, R.S.; Alencar, N.L.M.; Costa, J.H.; Prisco, J.T.; Gomes-Filho, E. Exogenous nitric oxide improves salt tolerance during establishment of *Jatropha curcas* seedlings by ameliorating oxidative damage and toxic ion accumulation. *J Plant Physiol* **2017**, *212*, 69-79, doi:10.1016/j.jplph.2017.02.005.
95. Reubens, B.; Achten, W.M.J.; Maes, W.H.; Danjon, F.; Aerts, R.; Poesen, J.; Muys, B. More than biofuel? *Jatropha curcas* root system symmetry and potential for soil erosion control. *J Arid Environ* **2011**, *75*, 201-205, doi:10.1016/j.jaridenv.2010.09.011.
96. Fairless, D. The little shrub that could - maybe. *Nature* **2007**, *449*, 652-655.
97. Arockiasamy, S.; Kumpatla, J.; Hadole, S.; Yepuri, V.; Patil, M.; Shrivastava, V.; Rao, C.; Kancharla, N.; Jalali, S.; Varshney, A.; et al. Breeding and biotechnological efforts in *Jatropha curcas* L. for sustainable yields. *Oil Crop Sci* **2021**, *6*, 180-191, doi:10.1016/j.ocsci.2021.10.004.
98. Souza, M.C.P.; Silva, M.D.; Binneck, E.; Cabral, G.A.L.; Iseppon, A.M.B.; Pompelli, M.F.; Endres, L.; Kido, E.A. RNA-Seq transcriptome analysis of *Jatropha curcas* L. accessions after salt stimulus and unigene-derived microsatellite mining. *Ind Crop Prod* **2020**, *147*, 112168, doi:10.1016/j.indcrop.2020.112168.
99. Mendes, K.R.; Batista-Silva, W.; Dias-Pereira, J.; Pereira, M.P.S.; Souza, E.V.; Serrão, J.E.; Granja, J.A.A.; Pereira, E.C.; Gallacher, D.J.; Mutti, P.R.; et al. Leaf plasticity across wet and dry seasons in *Croton blanchetianus* (Euphorbiaceae) at a tropical dry forest. *Sci Rep* **2022**, *12*, 954, doi:10.1038/s41598-022-04958-w.
100. Karnovsky, M.J. A formaldehyde-glutaraldehyde fixative of high osmolality for use in electron microscopy. *J Cell Biol* **1965**, *27*, 137-138.
101. Pompelli, M.F.; Martins, S.C.; Celin, E.F.; Ventrella, M.C.; DaMatta, F.M. What is the influence of ordinary epidermal cells and stomata on the leaf plasticity of coffee plants grown under full-sun and shady conditions? *Braz J Biol* **2010**, *70*, 1083-1088.
102. Lin, Y.K.; Huang, C.F. Stochastic flow network reliability with tolerable error rate. *Qual Technol Quant Manag* **2013**, *10*, 57-73, doi:10.1080/16843703.2013.116733.